

An examination of magnetized outflows from active galactic nuclei in galaxy clusters

P. M. Sutter¹ *, H.-Y. Karen Yang², P. M. Ricker², G. Foreman², and D. Pugmire³

¹*Department of Physics, University of Illinois at Urbana-Champaign, Urbana, IL 61801-3080*

²*Department of Astronomy, University of Illinois at Urbana-Champaign, Urbana, IL 61801*

³*Oak Ridge Leadership Computing Facility, Oak Ridge National Laboratory, Oak Ridge TN 37831*

10 June 2022

ABSTRACT

We present 3D adaptive mesh refinement MHD simulations of an isolated galaxy cluster that include injection of kinetic, thermal, and magnetic energy via a central active galactic nucleus (AGN) in order to study and evaluate the role that AGN may play in producing the observed cluster-wide magnetic fields. Using the MHD solver in FLASH 3.3, we compare several sub-resolution approaches to the evolution of AGN, specifically focusing on large-scale jet and bubble models. We examine the effects of magnetized outflows on the accretion history of the black hole and cluster thermodynamic properties, discuss the ability of various models to magnetize the cluster medium, and assess the sensitivity of these models to their underlying subgrid parameters. We find that magnetized jet-based models suffer a severe reduction in accretion rate compared to hydrodynamic jets; however, bubble models remain largely unaffected. While both jets and sporadically-placed bubbles have difficulty reproducing the observed strength and topology of cluster magnetic fields, models based on centrally-located bubbles come closest to observations. Finally, whereas jet models are relatively insensitive to changes in their subgrid parameters, the accretion rate and average magnetic field produced by the bubbles vary by as much as an order of magnitude depending on the grid resolution and accretion strength.

Key words: methods: numerical, MHD, galaxies: clusters: intracluster medium, galaxies: magnetic fields, galaxies: active

1 INTRODUCTION

Radio observations of clusters of galaxies indicate that they host large-scale, volume-filling diffuse magnetic fields of strength $0.1 - 10 \mu\text{G}$, while additional rotation measure observations suggest that these fields are tangled with auto-correlation lengths of 10-20 kpc (see Carilli & Taylor (2002) for a review) and have complex topology (Falceta-Gonçalves et al. 2010b). These fields are extremely important in understanding cluster astrophysics: they provide a source of non-thermal pressure support (Dolag & Schindler 2000), allow for synchrotron emission from cosmic rays (Miniati et al. 2001; Pfrommer et al. 2007; Brunetti et al. 2007; Skillman et al. 2008), potentially suppress or modify thermal conduction (Balbus 2000, 2001; Parrish et al. 2009), and modify turbulence in the cluster atmosphere (Narayan & Medvedev 2001; Chandran & Maron 2004; Shukurov et al. 2006). However, despite their ubiquity and importance we do not at

present understand their origins and evolution or the precise correlations of these fields with other cluster properties.

While exotic processes in the early universe may generate these large-scale fields (e.g., Baym et al. 1996; Bamba et al. 2008; Battefeld et al. 2008), magnetic fields may have difficulty surviving the radiation-dominated era due to very high diffusion rates (Lesch & Birk 1998). Alternatively, we may turn to astrophysical mechanisms, and especially active galactic nuclei (AGN), for seeding and amplifying magnetic fields. In this scenario, weak seed fields ($\sim 10^{-18}$ G) are generated via a plasma process, such as the Biermann battery mechanism (Biermann 1950; Widrow 2002). Dynamo action in supermassive black hole (SMBH) accretion disks can quickly amplify these weak fields and expel them into the intracluster medium via relativistic jets (Koide et al. 1999). The jets can propagate tens of kiloparsecs into the intracluster medium (Kirkpatrick et al. 2011) and inflate bubbles when these jets slow and reach approximate pressure balance with their surroundings (Colbert et al. 1996). The bubbles rise into the intracluster medium (ICM) and eventually disperse, distributing heat (Voit & Donahue 2005)

* Email: psutter2@illinois.edu

and potentially magnetic fields within cluster cores. AGN outflows are more than powerful enough to match the observed magnetic energy in clusters (Colgate & Li 2000) and are natural carriers of magnetic flux (Daly & Loeb 1990). Rotation measure observations of jets indicate the presence of magnetic fields in them (Contopoulos et al. 2009). AGN feedback is also a strong candidate for preventing excessive cooling in cluster cores (McNamara & Nulsen 2007).

However, the complex physics of AGN accretion disks and jets coupled with the small scales involved (~ 100 pc) makes it difficult to include AGN in cluster and cosmological simulations, which typically resolve scales greater than 2 kpc. Thus, we must include the accretion and feedback processes as subgrid models. Subgrid models have been developed and employed by many authors with varying levels of sophistication. Accretion rate calculations can vary from the simple Bondi rate (Bondi 1952) to estimates of viscous angular momentum transport (Debuhr et al. 2010) to fully stochastic models (Pope 2007). If the resolution and computing resources permit it, large-scale jets can be placed on the simulation grid with many modifications, including simple fluxes at cell boundaries (Gaspari et al. 2011), limited-lifetime jets (Morsony et al. 2010), extended jets (Cattaneo & Teyssier 2007), wide-angle jets (Sternberg et al. 2007), and precessing jets (Sternberg & Soker 2008; Falceta-Gonçalves et al. 2010a). Since jets eventually inflate bubbles, it is easier computationally to simply place already-formed bubbles (e.g., Sijacki et al. 2007; Gardini 2007; Di Matteo et al. 2008; Booth & Schaye 2009) or to slowly inflate them (e.g., Jones & De Young 2005). Whereas jets continuously feed back energy and momentum onto the simulation grid, bubbles are modeled as discrete events.

All of the above models have been discussed using purely hydrodynamic simulations. While there has been some research into the effects of AGN-driven turbulence in a magnetized cluster (Dubois et al. 2009), magnetized outflows themselves have only been studied by a few authors. The stability of AGN-blown bubbles with a predetermined magnetic field configuration has been somewhat well examined (e.g., Robinson et al. 2004; Jones & De Young 2005; Ruszkowski et al. 2007; Dursi & Pfrommer 2008; Xu et al. 2008; Gourgoulatos et al. 2010). Additionally, Xu et al. (2010) and O’Neill & Jones (2010) have followed the evolution of magnetized jets and bubbles in the cosmological formation of a large cluster. However, no simulations of magnetized AGN outflows have included feedback processes coupled to their surroundings; these studies have presumed a fixed energy in the magnetized bubbles. This link between the feedback energy and the accretion rate is essential in order to reproduce the observed cosmic SMBH mass density (Hopkins et al. 2006) and the correlation between SMBH mass and galactic bulge velocity dispersion (Booth & Schaye 2009). Furthermore, there has been no systematic comparison study of the various models of AGN feedback when magnetic energy is included (see Dubois et al. (2011) and our companion paper, Yang et al. (2011), for a comparison study of purely hydrodynamic outflows).

In this work, we use FLASH MHD simulations of a mock isolated cluster to examine several different AGN subgrid models, exploring variations of their parameters for a variety of resolutions (we have independently studied subgrid models of SMBH formation and merging in Sutter & Ricker

(2010)). Since we cannot perform an exhaustive study of all the models presented above, we select a representative bubble model (Sijacki et al. 2007) and a representative jet model (Cattaneo & Teyssier 2007). We add the magnetic field injection model of Li et al. (2006). We perform a systematic study of these models by varying some of the parameters available for each model in otherwise identical simulation setups. Note that for this study, we do not evaluate the models in terms of their respective abilities to reproduce cluster observables; our goal in this manuscript is to take the models as read in their respective papers and apply magnetic injection to them. By choosing jet and bubble models we are able to compare and contrast continuous, centrally located small-volume injections (jets) with sporadic, randomly located large-volume injections (bubbles). We also vary the parameters associated with accretion rate models, since these are tightly coupled to the feedback properties and hence the resulting magnetic field. We choose to simulate both bubble and jet models because they are very distinct: they differ in the form of injected hydrodynamic energy, the shape of the injection region, and the periodicity of feedback events. These two approaches allow us to bracket a wide range of plausible feedback models and explore the roles that their injected magnetic fields can play in the evolution of their host clusters.

We have three main goals in this work: to examine the effect that introducing magnetic fields into the AGN injection region has on the accretion and feedback properties of the SMBH, to evaluate the ability of the various studied models to magnetize an initially unmagnetized cluster, and to examine the robustness of these models to changes in their subgrid parameters. We will characterize the resulting magnetic fields in terms of field morphology, growth rates, and radial profiles. We begin with a discussion of our simulation code and mock cluster setup in Section 2 and a description of the subgrid models we study in Section 3. We examine the role that magnetic fields play in modifying the feedback properties of the modeled AGN in Section 4 and the ability of our fiducial jet and bubble models to magnetize a cluster in Section 5. We then examine the magnetic topology of the produced fields for the fiducial runs via streamlines and rotation measure maps in Section 6. Finally, we perform a parameter survey in Section 7. For this survey, we focus mainly on the changes to the accretion rate and magnetic properties of the outflows. We conclude and offer recommendations for constructing reliable subgrid models in Section 8.

2 NUMERICAL APPROACH

Using the adaptive mesh refinement code FLASH 3.3 (Fryxell et al. 2000; Dubey et al. 2008), we performed three-dimensional magnetohydrodynamic simulations with radiative cooling and AGN feedback within an isolated mock cluster sitting in a 2048 kpc box. We constructed the mock cluster gas using an ideal-gas equation of state in hydrostatic equilibrium with an NFW gravitational profile (Navarro et al. 1996). We assumed a cluster mass of $1.5 \times 10^{14} M_{\odot}$, concentration 5.53, gas fraction 0.1, and Hubble constant $h = 0.65$. For computing accretion and feedback properties, we placed a $3 \times 10^9 M_{\odot}$ black hole in the cluster center. Note that we did not include the black hole mass in the

computation of the gravitational potential. We computed radiative cooling rates using the collisional ionization equilibrium tables of Sutherland & Dopita (1993) assuming 1/3 solar metallicity. This is the same cluster as used in the analysis of Cattaneo & Teyssier (2007), and is motivated by observations of M87.

We maintained a minimum resolution of 32 kpc throughout the simulation volume and enabled progressive nested refinement centered on the black hole. We varied the peak refinement (see below) from 0.5 to 16 kpc. We defined the maximally-refined region as a box of width 80 kpc for jets and 160 kpc for bubbles. We did not include any other refinement criteria.

3 SUBGRID MODELS

3.1 Accretion rate

The most basic component of the accretion model is the black hole mass. While this mass will change with time as gas accretes onto the SMBH, we must select an initial seed value. The accretion rate is strongly dependent on mass, and hence the the feedback energies in the early cluster evolution can vary greatly. Ideally, we would perform cosmological simulations and include the formation and evolution of black holes along with our simulated clusters (e.g., Booth & Schaye 2009; Sutter & Ricker 2010). Since we are simulating an already-formed mock cluster, we must select some value. While some authors (e.g., Sijacki et al. 2007) have placed low-mass ($\sim 10^5 M_\odot$) black holes in massive clusters to study their growth, this is not consistent with the known $M_{\text{bh}} - M_{\text{tot}}$ relation (Bandara et al. 2009). We will choose a value consistent with an already-formed cluster, $M_{\text{bh}} = 3 \times 10^9 M_\odot$.

For the purposes of this study, we restrict our survey to the somewhat simple, but widely used, so-called α -model of estimating the SMBH accretion rate. The α -model is a simple modification to the Bondi-Hoyle-Lyttleton (Bondi 1952) accretion rate:

$$\dot{M}_{\text{Bondi}} = 4\pi G^2 M_{\text{bh}}^2 \frac{\rho}{c_s^3}, \quad (1)$$

where the sound speed c_s and the density ρ are measured on the simulation mesh, and M_{bh} is the black hole mass. This approximates well the observed accretion rate when the Bondi rate is measured at parsec scales (Allen et al. 2006). However, simulations of clusters and larger structures cannot obtain sufficient resolution to reach these parsec scales, so we must include some compensating factor. If we assume that we are underestimating the true accretion rate at the scales we typically resolve, we can simply multiply the calculated Bondi rate by a constant:

$$\dot{M}_{\text{bh}} = \alpha \dot{M}_{\text{Bondi}}. \quad (2)$$

We are free to choose the value of α , and we will examine values from 1 (i.e., regular Bondi accretion) to 300, both at fixed resolution and by allowing the α parameter to scale with resolution, under the assumption that as we lower the resolution we must make greater enhancements to the calculated Bondi rate. While more sophisticated alternatives exist, such as the β -model of Booth & Schaye (2009) or the stochastic model of Pope (2007), we currently do not have

Table 1. Parameters of the accretion rate model.

Parameter	Description	Value(s)
M_{bh}	Initial BH mass (M_\odot)	3×10^9
α	Bondi multiple	1 – 300
\dot{M}_{max}	Maximum accretion rate	\dot{M}_{Edd}
R_{acc}	Accretion radius (zones)	1 – 4
R_{dep}	Minimum depletion radius (zones)	1 – 4
f_{dep}	Maximum gas depletion fraction	0.1

a complete understanding of the complex physics involved in accretion flows. Hence, for this study we will keep this portion of the subgrid model as simple as possible.

We must also choose the region in our simulation mesh where we will measure the density and sound speed for computing the accretion rate. While we may simply sample the immediate zones around the SMBH, this approach may suffer from undue variability, especially in the case of jet-based feedback where the primary effects of the feedback are felt in those same zones. However, if we choose too large a radius, we will poorly sample the gas properties and incorrectly estimate the accretion rate.

Similarly, we must remove gas from the simulation mesh as we accrete it onto the black hole. As before, we have the freedom to choose from where we will remove the gas. If we choose too small a depletion region, then in the case of strong accretion events we may potentially remove too much gas from the central zones, leading to numerical instability. On the other hand, removing gas from zones far away from the SMBH is clearly unphysical, since this gas does not actually accrete onto the black hole. To achieve a balance, many authors (e.g., Dubois et al. 2010) choose a minimum gas removal threshold so that the size of the depletion region is chosen to ensure that no more than some fraction of the gas in the depleted cells (for example, 10%) is removed in any one timestep.

Since the accretion rate is proportional to the gas density and the gas density is directly affected by our depletion mechanism, our choices for the accretion and depletion regions influence each other and thereby the feedback properties of the AGN. We include in our study a spherical region with radius 1 to 4 zones, varying the accretion and depletion radii jointly and separately. We also maintain a maximum depletion fraction of 10% with the *minimum* depletion radius set as described above.

For all accretion models, we impose an upper limit on the accretion rate corresponding to the Eddington rate,

$$\dot{M}_{\text{Edd}} = \frac{4\pi G M_{\text{bh}} m_p}{\epsilon_f \sigma_T c}, \quad (3)$$

where m_p is the mass of the proton, σ_T is the Thompson cross-section, and ϵ_f is the radiative efficiency.

In Table 1 we summarize the parameters included in the accretion rate model and the values included in our survey: the initial black hole mass M_{bh} , the Bondi multiple α , the maximum accretion rate \dot{M}_{max} , the accretion radius R_{acc} , the minimum depletion radius R_{dep} , and the maximum gas depletion fraction, f_{dep} .

3.2 Jet-based feedback

We follow the general prescription of Cattaneo & Teyssier (2007) for building our jet-based feedback models. This particular model does not simulate the relativistic jet immediately after its launch from the AGN accretion system, which we do not have the resolution to accurately simulate, but rather the large-scale non-relativistic outflow as the jet extends to kpc scales and begins to entrain ICM material. This jet imparts thermal and kinetic energy to the ICM as well as a small amount of mass fed back from the accretion disk.

The injection rates of the mass, momentum, and energy onto the grid are treated as source terms in the hydrodynamic equations, where the energy injection rate is

$$\dot{E} = \epsilon_f \dot{M}_{\text{bh}} c^2 (1 - \eta) |\Psi|. \quad (4)$$

Similarly, the momentum injection rate is $\dot{\mathbf{P}} = \sqrt{2\epsilon_f} \dot{M} c \Psi$, and the mass injection rate is $\dot{M}_{\text{inj}} = \eta \dot{M} |\Psi|$. In the above, ϵ_f is a feedback efficiency and η is the jet mass loading factor, which is a parameterization of the entrainment of gas as the jet propagates. A jet mass loading factor of $\eta = 1$ corresponds to the case in which there is no entrainment and the feedback energy is entirely kinetic. Higher values allow for the deposition of thermal energy.

The window function Ψ , which provides a mapping onto the mesh, is

$$\Psi(\mathbf{x}) = \frac{1}{2\pi r_{\text{ej}}^2} \exp\left(-\frac{x^2 + y^2}{2r_{\text{ej}}^2}\right) \frac{z}{h_{\text{ej}}}. \quad (5)$$

We cut off injection at $z = h_{\text{ej}}$ and $r = r_{\text{ej}}$. Note that we normalize the injected energy within the window function by dividing Ψ by its integral $\|\Psi\| = 1 - \exp(-0.5r_{\text{ej}}^{-2})$. The injection region is oriented along the z -axis. There is no threshold associated with activating jet feedback; the jet operates continuously, as suggested by observations (Peterson & Fabian 2006).

Note that our specific implementation differs in several ways from that of Cattaneo & Teyssier (2007). First, we normalize our value of Ψ . Subsequent papers based on the same model, such as Dubois et al. (2010), do this as well. Also, their model fixed the mass of the SMBH for purposes of calculating the accretion rate. For jets, this is a reasonable approximation, since the accretion rate does not reach high values. We also simulate a larger volume and maintain a larger maximally-refined central region. Furthermore, we use a smaller R_{acc} and allow depletion of gas from the ICM. When accounting for all these differences we have been able to match their results.

As do Cattaneo & Teyssier (2007) we fix the values of $\eta = 100$ and $\epsilon_f = 0.1$, which are chosen to match observed jet velocities. We vary the jet size, both exploring larger jets with fixed resolution and maintaining a fixed ratio of jet to grid size. While larger jets may be somewhat unphysical, in cosmological simulations we can only reach resolutions of $\Delta x \sim 2\text{--}4$ kpc, and so this may be the only option available. While a jet height of 0 is a valid model, corresponding to a simple flux at a cell boundary, we will not study it here since we require some spatial extent for the injection of magnetic flux (see below).

Table 2 summarizes the aspects of the jet model and our chosen values: the feedback efficiency ϵ_f , the jet mass loading factor η , the jet height h_{ej} , and jet radius r_{ej} .

Table 2. Parameters of the jet-based feedback model.

Parameter	Description	Value(s)
ϵ_f	Feedback efficiency	0.1
η	Jet mass loading factor	100
h_{ej}	Jet height (kpc)	2 – 16
r_{ej}	Jet radius (kpc)	2.5 – 20

3.3 Bubble-based feedback

For bubble-based feedback we follow the method outlined in Sijacki et al. (2007), which places over-pressurized bubbles displaced from the SMBH location. In their model we have only thermal energy injection:

$$\dot{E} = \epsilon_m \epsilon_f c^2 \Delta M_{\text{bh}}, \quad (6)$$

where ΔM_{bh} is the increase in BH mass since the last bubble event, ϵ_f is the feedback efficiency and ϵ_m is the mechanical heating efficiency. We distribute this energy on a per-mass basis in a sphere with radius determined by

$$R_{\text{bub}} = R_0 \left(\frac{\dot{E} \Delta t \rho_0}{E_0 \rho} \right)^{1/5}, \quad (7)$$

where we define the radial scaling $R_0 = 30 h^{-1}$ kpc, energy scaling $E_0 = 10^{55}$ ergs, density scaling $\rho_0 = 10^4 h^{-2} M_{\odot} \text{ kpc}^{-3}$, Δt is the time since the last bubble injection event. These scalings are chosen to ensure that a bubble in a typical cluster environment will have a realistic size when it has reached pressure equilibrium with the ICM. We have used the same values as in the cosmological runs of Sijacki et al. (2007). Since bubble events are episodic, we must select some criterion for forming bubbles. We only form bubbles when the black hole has increased its mass since the previous bubble event by $\Delta M_{\text{bh}}/M_{\text{bh}} > 0.01\%$, which was chosen by Sijacki et al. (2007) to produce the observed $M_{\text{bh}} - \sigma$ relation.

Since observed bubbles are displaced away from the cluster centers (e.g., Voit & Donahue 2005), we randomly place each bubble with a maximum displacement R_{dis} equal to the calculated bubble radius R_{bub} . However, we also examine the case in which we fix the bubble radius at 40 kpc and do not displace the bubble centers away from the central SMBH, as has been used in several cosmological simulations (e.g., Di Matteo et al. 2008; Battaglia et al. 2010). This setup should be an intermediate case between bubbles and jets.

In Table 3 we summarize our bubble model parameters and the values we examine in our survey: the minimum black hole mass increase to trigger a bubble event Δ_{bh} , the feedback efficiency ϵ_f , the mechanical heating efficiency ϵ_m , the bubble radial scale R_0 , the bubble energy scale E_0 , the bubble density scale ρ_0 , and finally the maximum displacement of the bubble center R_{dis} .

As opposed to the jet feedback mechanisms, which as we will see maintain low accretion rates due to the more concentrated heating of the core, episodic bubble-based models can occasionally allow the accretion rate to reach large fractions of the Eddington rate. Indeed, observations indicate that the SMBH accretion rate is very high, at least at high redshift (Fan 2006). When the accretion rate, and hence the

Table 3. Parameters of the bubble-based feedback model.

Parameter	Description	Values(s)
Δ_{bh}	BH mass increase	0.01%
ϵ_f	Feedback efficiency	0.1
ϵ_m	Mechanical heating efficiency	0.2
R_0	Radial scale (h^{-1} kpc)	30
E_0	Energy scale (ergs)	10^{55}
ρ_0	Density scale ($h^{-2} M_{\odot} \text{ kpc}^{-3}$)	10^4
R_{dis}	Maximum center displacement	$0.0 - R_{\text{bub}}$

Table 4. Parameters of the quasar-based feedback model.

Parameter	Description	Value(s)
χ_{radio}	Two-mode feedback threshold	$0.01 \dot{M}_{\text{Edd}}$
ϵ_f	Feedback efficiency	0.1
ϵ_r	QSO heating efficiency	0.05
R_{radio}	Feedback radius (zones)	8

available feedback energy, reaches large values the feedback takes the form of pure radiation (Fender et al. 1999; Gallo et al. 2003). In this case, instead of mechanically inflating bubbles, the outflows from the AGN simply heat the nearby gas:

$$\dot{E} = \epsilon_f \epsilon_r c^2 \dot{M}, \quad (8)$$

where ϵ_f is the feedback efficiency and ϵ_r is the QSO heating efficiency. We must choose a threshold to switch to this feedback mode, and we follow Sijacki et al. (2007) with a value of $0.01 \dot{M}_{\text{Edd}}$. We are free here to choose our radius for depositing the energy, and for numerical stability we choose a feedback radius of 8 zones.

Table 4 lists the parameters and values for the quasar-mode feedback: the two-mode feedback threshold χ_{radio} , the feedback efficiency ϵ_f , the QSO heating efficiency ϵ_r , and the radius of feedback R_{radio} . We fix all these values and do not include any variance in our parameter survey here.

3.4 Magnetic field injection

We take the form of injected magnetic fields to be the ‘‘tower’’ model of Li et al. (2006), which assumes an underlying collimated jet extending away from the accretion system:

$$B_r(r', z') = 2B_0 z' r' \exp(-r'^2 - z'^2) \quad (9)$$

$$B_z(r', z') = 2B_0 (1 - r'^2) \exp(-r'^2 - z'^2) \quad (10)$$

$$B_\phi(r', z') = B_0 \alpha_B r' \exp(-r'^2 - z'^2), \quad (11)$$

where $r' = \sqrt{x^2 + y^2}/r_0$ and $z' = z/r_0$. Here, we set the scale radius r_0 to be $0.5R_{\text{inj}}$, so that $r_0 = 0.5R_{\text{bub}}$ for bubbles and $r_0 = 0.5R_{\text{ej}}$ for jets, so that the entire injected magnetic structure fits inside the given feedback region. The magnetic field injected via the above prescription is constructed so that it has zero divergence, and this scaling ensures that we minimize divergences caused by the artificial cutoff. α_B is the ratio of poloidal to toroidal flux, which we

Table 5. Parameters of the magnetic injection model.

Parameter	Description	Values(s)
r_0	Radial scale	$1/2r_{\text{inj}}$
α_B	Poloidal/toroidal ratio	$\sqrt{10}$
E_B	Fraction of total energy in B	$0.0 - 1.0$

choose to be $\alpha_B = \sqrt{10}$ for a field with minimum initial Lorentz force, as suggested by Li et al. (2006). We determine the scale B_0 by giving some fraction of the available feedback energy to the magnetic field: either 0.0 for purely hydrodynamic outflows, 0.5 for an equipartition case, or 1.0 for purely magnetic outflows. Note that for purely magnetic outflows in jets, we ignore the details of the window function Ψ in Eq. 5 and use it simply to determine the extent of the magnetic feedback region. For jet models, we align the axis of the magnetic field with the axis of the jet, and for bubbles we align the magnetic field axis with a vector pointing from the bubble center to the position of the SMBH.

We summarize the parameters of our magnetic field injection in Table 5: the radial scale r_0 , the ratio of poloidal to toroidal flux α_B , and the fraction of feedback energy available to magnetic fields E_B . Aside from the energy of the magnetic injection, we do not vary these parameters.

3.5 Parameter survey

In Tables 6 and 7 we detail our parameter survey for jets and bubbles, respectively. We only include in the tables those parameters that we vary in our survey. We have collected each set of parameter changes into several groups. Each group is given a unique numerical identifier, and each set of parameters within that group is given an alphabetical label. For later plots, we label purely hydrodynamic simulations as ‘‘h’’, equipartition models (i.e., $E_B = 0.5E_{\text{tot}}$) as ‘‘e’’, and purely magnetic feedback runs as ‘‘m’’. Thus, the label ‘‘J3Bm’’ will designate purely magnetic outflow (‘‘m’’) from the second parameter set (‘‘B’’) of the third grouping (‘‘3’’) of the jet models (‘‘J’’).

For jets, in our first group we study changing the peak grid resolution with a fixed jet size of $h_{\text{ej}} = 2.5$ kpc and $r_{\text{ej}} = 2.0$ kpc. In the next group we also vary the resolution but allow the jet size to scale with the resolution such that $h_{\text{ej}} = 5$ zones and $r_{\text{ej}} = 4$ zones. In the third group we vary the accretion strength α . Finally, in the last group we investigate the effects of changing the accretion and depletion radii on the resulting feedback. We do this because the jet model as described in (Cattaneo & Teyssier 2007) does not include any gas depletion, and changing these values can have significant consequences for jets since the feedback is applied very close to the central black hole. Note that for most of the jet groups we do not use our peak resolution of 0.5 kpc, but rather the larger 1.0 kpc. We chose this so that we would have enough computational resources to complete the study. We only include equipartition magnetic fields in the first group, where we vary the grid resolution. Note that the model set ‘‘J1B’’ serves as our fiducial jet case.

For the first group of our bubble model survey, we vary the resolution while keeping the other bubble parameters fixed. Since the bubbles are much larger than the jets (50-

Table 6. Jet model parameter survey.

Designation	Δx (kpc)	α	h_{ej} (kpc)	r_{ej} (kpc)	$R_{\text{acc}}/\Delta x$	$R_{\text{dep}}/\Delta x$
Varying Resolution						
J1A	0.50	1	2.0	2.5	2.0	2.0
J1B	1.00	-	-	-	-	-
Scaling Jet Size with Resolution						
J2A	-	-	4.0	5.0	-	-
J2B	2.00	-	8.0	10.0	-	-
J2C	4.00	-	16.0	20.0	-	-
J2D	-	-	8.0	10.0	-	-
Varying Alpha						
J3A	0.50	100	2.0	2.5	-	-
J3B	1.00	-	-	-	-	-
J3C	-	300	-	-	-	-
Varying Accretion and Depletion Radii						
J4A	-	1	-	-	1.0	1.0
J4B	-	-	-	-	4.0	4.0
J4C	-	-	-	-	2.0	0.0

200 kpc), we may lower our resolution much more than in the jet runs. In the next two groups we vary the accretion multiple α both with fixed resolution and by scaling α with the grid resolution. For our last group, we fix the bubble position on the SMBH. Note that for this case, we also fix the bubble radius to $R_0 \approx 40$ kpc. This represents an intermediate case between jets and bubbles and is used frequently in cosmological simulations (e.g., Di Matteo et al. 2008; Battaglia et al. 2010). We include the equipartition magnetic feedback mode only with the bubble run (“B1B”) which is at the same resolution as the jet runs, and for the fixed bubble run. We do not examine the role that the accretion and depletion radii play in this bubble survey, since the bubble feedback is not as sensitive to these criteria. Note that the model set “B1B” serves as our fiducial bubble case.

4 THE EFFECTS OF MAGNETIC INJECTION ON AGN FEEDBACK

Before we fully examine the growth and structure of magnetic fields using the models described above, we must first see what, if any, effects the presence of injected fields has on the accretion and feedback properties of the AGN as well as on some of the resulting hydrodynamic characteristics of the cluster medium. We choose three of our models to examine: J1B and B1B, representing our fiducial cases for jets and bubbles, respectively, and model B4A, which uses bubbles with fixed centers and radii. For each model we examine purely hydrodynamic injection, fully magnetic injection, and an intermediate equipartition case in which the available injection energy is evenly split between magnetic and hydrodynamic components. For the plots below, models J1B and B1B have plot titles of “Jets” and “Bubbles”, respectively, while model B4A is called “Fixed Bubbles.”

Table 7. Bubble model parameter survey.

Designation	Δx (kpc)	α	$R_{\text{dis}}/R_{\text{bub}}$
Varying Resolution			
B1A	0.50	1	1.0
B1B	1.00	-	-
B1C	2.00	-	-
B1D	4.00	-	-
B1E	8.00	-	-
Varying Alpha			
B2A	2.00	100	-
B2B	-	300	-
Scaling Alpha with Resolution			
B3A	0.50	50	-
B3B	4.00	300	-
Fixing Bubble Position			
B4A	1.00	1	0.0

Figure 1 shows the black hole accretion rate as a fraction of the Eddington limit ($\dot{M}/\dot{M}_{\text{Edd}}$) for the jet model. We find that simply the presence of an injected magnetic field drastically reduces the accretion rate: for ~ 3 Gyr the magnetic fields suppress the accretion rate by a factor of five, with much smaller differences between the equipartition and fully magnetic runs. This has two causes. First, the shape of the magnetic injection, which is initially a torus rather than the axial jet of the hydrodynamic feedback, does some-

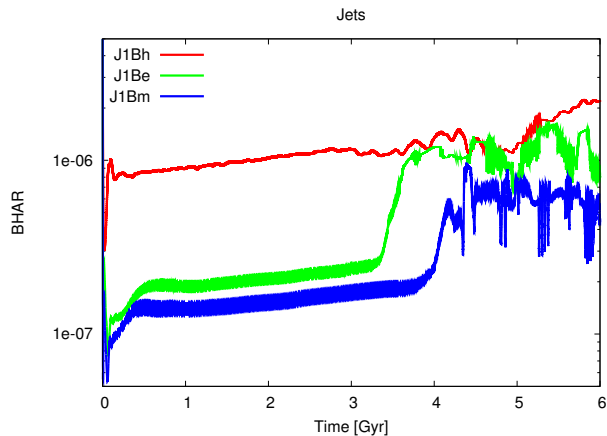


Figure 1. Effects of magnetic injection on the black hole accretion rate. Shown is BHAR ($\dot{M}/\dot{M}_{\text{Edd}}$) versus time for purely hydrodynamic, equipartition, and fully magnetic modes of the J1B (Jets) model

what prevent accretion onto the black hole. However, we performed tests where we injected thermal energy with the same distribution as the magnetic injection and found only small differences. The main cause of the reduced accretion rate is the “unspringing” of the highly tense injected fields. As the fields unfold after injection they efficiently drive gas away from the central zones. Eventually, however, the gas is able to cool sufficiently and overcome this tension and the accretion rate correspondingly jumps. However, the magnetized outflows still maintain an accretion rate a factor of two lower than in the purely hydrodynamic case. The accretion rate for the magnetized cases is also highly variable with a short characteristic timescale of 1-10 Myr. This is indicative of the complex relationship between the unfolding magnetic fields and the gas which is attempting to accrete onto the black hole.

After 6 Gyr, the purely hydrodynamic mode undergoes a period of intense activity characterized by a rapid rise in accretion rate as the gas cools sufficiently and an associated enhanced feedback phase (see Cattaneo & Teyssier 2007). At this point the strong magnetic fields in the core become highly tangled, and the combination of strong fields surrounding the core and cold, dense gas at the core results in very low plasma β values and hence severely lowers our magnetohydrodynamical timestep. Thus we can not efficiently carry the simulation further and simultaneously perform our intended parameter survey. For this run and all others, we evolve the simulations until the timestep drops too low to continue effectively. However, we are still able to perform these simulations across billions of years, and the timing of the onset of complex fields can yield useful information about the relationship between the magnetic fields and the cluster gas.

The effects of the injected magnetic field are much less pronounced in the randomly-placed bubble model (B1B), as highlighted by bubble size as a function of time, as shown in Figure 2 (note that the other bubble model examined here, B4A, uses a fixed bubble radius, and thus is not shown). The bubbles in all cases start out very large, with radii nearly 200 kpc. Over 4 Gyr they grow smaller and

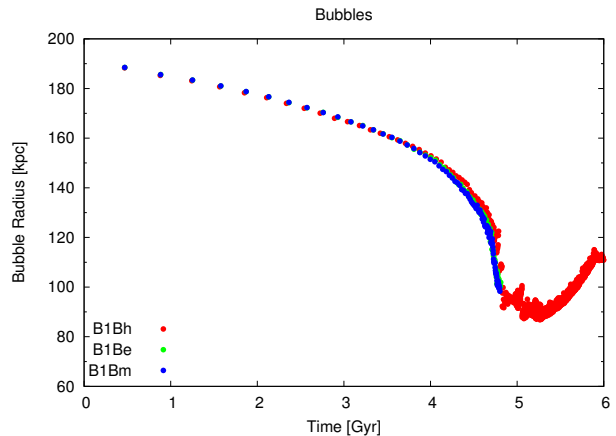


Figure 2. Effects of magnetic injection on the bubble size. Shown is bubble radius at each injection event as a function of time for model B1B.

more frequent as the time between injection events grows shorter and the core density increases (which we will discuss in detail later). Eventually the hydrodynamic bubbles begin to exhibit periodic behavior, but the magnetic fields become too complex to follow efficiently at this resolution. This also means that the accretion rate is much less affected, as shown in Figure 3. Since the bubbles are large and off-centered, the magnetic fields are not as effective at driving away gas from the core, and hence the accretion histories of the three modes (purely hydrodynamic, equipartition, and purely magnetic) are nearly identical (for a discussion of the differences in accretion rate with and without feedback, see our companion paper Yang et al. 2011). Additionally, there is almost no difference between the equipartition and fully magnetic modes. The hydrodynamic injections are eventually able to reach the two-mode feedback threshold.

When we force the bubbles to be centered on the black hole, as with model B4A, we achieve similar suppression of the accretion rate as for the jets, as we see in Figure 3. These differences take ~ 3 Gyr to manifest, however, since the bubbles are larger than the injection region and hence not as efficient as the jets at driving away gas (this is also noticeable when comparing the purely hydrodynamic modes, where the jets have an accretion rate roughly an order of magnitude smaller than the bubbles). Once again we also see the importance of merely the presence of magnetic injection over the relative strength of those fields: both the equipartition and fully magnetic modes exhibit nearly the same behavior, which after 3 Gyr is characterized by small (factor of ~ 2) changes to the accretion rate with a cyclic period of roughly 3 Gyr, whereas the hydrodynamic injections see much larger variations in the accretion rate over much smaller timescales.

We show radial profiles of the density in Figure 4. These are constructed from volume-averaged quantities in shells of thickness 1 kpc. For the jets we see that at 2 Gyr the magnetized injections are more effective at driving gas away from the core, but outside of the central regions of the cluster there are very few differences. However, after 6 Gyr the accreting gas pushes through the magnetic fields and the magnetized outflows end up with a slightly higher central

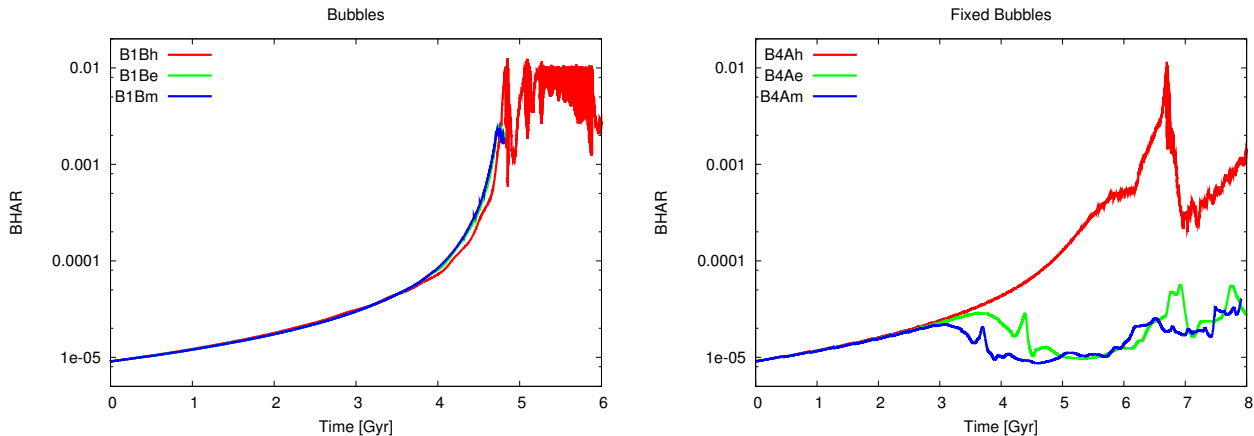


Figure 3. Effects of magnetic injection on the black hole accretion rate. Shown is BHAR ($\dot{M}/\dot{M}_{\text{Edd}}$) versus time for purely hydrodynamic, equipartition, and fully magnetic modes of models B1B (Bubbles), and B4A (Fixed Bubbles).

density, though once again the injection modes are indistinguishable past 20 kpc. Even though the density is higher in the magnetized runs, the sound speed is also higher, resulting in the reduced accretion rate discussed above.

The randomly-placed bubbles, as expected, also exhibit no differences between magnetized and unmagnetized profiles at 4 Gyr, whereas the fixed bubbles show remarkable differences out to a radius of 100 kpc. After this, the purely hydrodynamic bubbles significantly heat the core, which drives gas into the outer regions of the cluster atmosphere. At 4 Gyr the magnetized outflows have prevented large amounts of material from collapsing into the core and the equipartition mode has formed a low-density shell from 30 to 70 kpc. The purely hydrodynamic mode has a much smaller low-density shell at 70 kpc. For the hydrodynamic case the heated outwardly-expanding gas in the injection regions prevents further accretion of material from the rest of the cluster, while some of the inner material within the injection region falls towards the black hole. In the equipartition case the complex interplay of the magnetic fields and injected thermal energy forms a larger shell. For the fully magnetized outflow the magnetic fields simply drive gas away from the core. By 7 Gyr, however, the profiles have reversed: the intense activity of the hydrodynamic bubbles has driven gas away from the core (note that this profile is taken from a point in time which is at the trough in a cyclic pattern, as seen in Figure 3) while the more sedate magnetized injections see relatively little change in the density profiles.

These conditions are also reflected by the emission-weighted temperature, as we show in Figure 5. Note that we did not observe significant differences in the pressure profile and hence do not show them here. For the jets, the magnetic fields, which are much more effective at removing gas from the central core, heat up the gas to 3.5×10^7 K after 2 Gyr of evolution. Eventually the gas is able to cool, and in the magnetized case the gas reaches 10^7 K after 6 Gyr, about 30% lower than in the purely hydrodynamic case. This is also the case with the fixed bubbles, where initially the magnetized outflows maintain higher temperatures in the core relative to the thermal outflows, but after 7 Gyr the magnetic bubbles change the inner temperature by at most 20%, whereas the hydrodynamic bubbles heat the gas considerably.

5 THE GROWTH OF MAGNETIC FIELDS

To examine in detail the growth of magnetic fields, we will take only our fiducial cases J1B for the jets and B1B for the bubbles as well as the intermediate fixed bubble case of B4A. These three cases have the same peak resolution and accretion properties and - other than the form of the injection - these runs differ only in that the bubble runs use a larger centrally-refined region. For this section we only study fully magnetic injection, with no portion of the feedback energy in thermal or kinetic modes.

We first examine the rate of magnetic field injection, B_{inj} , in Figure 6. The jets (model J1B) inject magnetic fields continuously at a rate $\sim 600 \mu\text{G Myr}^{-1}$ for approximately 4 Gyr. Once the core begins to significantly cool down the accretion rate jumps and subsequently the jets become more powerful, seeding magnetic fields at an average rate of $1100 \mu\text{G Myr}^{-1}$. Periodic behavior also sets in with spikes of up to $8000 \mu\text{G Myr}^{-1}$ occurring every ~ 500 Myr. Since the feedback in this case takes place in the volume which is used to measure the accretion rate, the injected magnetic field rate is highly sensitive to small perturbations in the gas properties of this region, and thus is very noisy. Also, the total feedback magnetic energy is distributed over a much smaller volume than the bubbles, hence the higher magnetic field values.

Both bubble models require ~ 400 Myr before the first injection event takes place. While the fixed bubbles (model B4A) inject fields about 5 times stronger than the randomly-placed bubbles (model B1B), these injections take place within a fixed radius of 40 kpc, while the randomly-placed bubbles have radii of ~ 200 kpc initially. Thus while the injected energies are identical for the initial injection and roughly equal for the subsequent 4 Gyr, the randomly-placed bubbles distribute this energy over a large volume, and hence the magnetic field strength within that volume is lower. The fixed bubbles reach a peak injection rate of $700 \mu\text{G Myr}^{-1}$ before strong outflows prevent further accretion at 4 Gyr, which is roughly the same time when the jets begin their strong feedback phase. The randomly-placed bubbles, which take longer to drive gas away from the core, only reach a

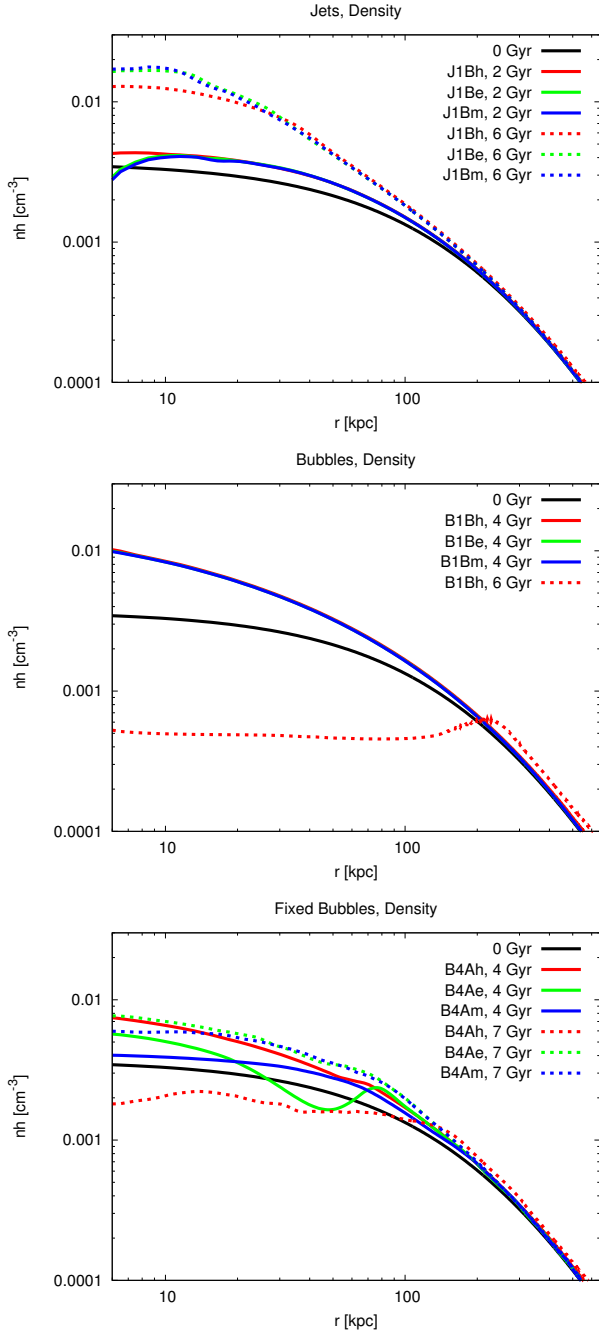


Figure 4. Effects of magnetic injection on the cluster density profile.

peak injection rate of $100 \mu\text{G Myr}^{-1}$ before the complex field topology prevents further efficient calculations.

We show in Figure 7 the average magnetic field strength within two radii, $R = R_{\text{core}} \equiv 0.15R_{500}$ and $R = R_{200}$. We take a density-weighted average in the core and a volume-weighted average for the entire cluster. The fixed bubbles are most efficient at strongly magnetizing the core, reaching $1 \mu\text{G}$ after just 1 Gyr, which is an order of magnitude stronger than the jets and randomly-placed bubbles, and a peak value of over $2 \mu\text{G}$ averaged inside the core after 4 Gyr. After that time the reduced accretion rate prevents further strengthening of the field in the core. At that time

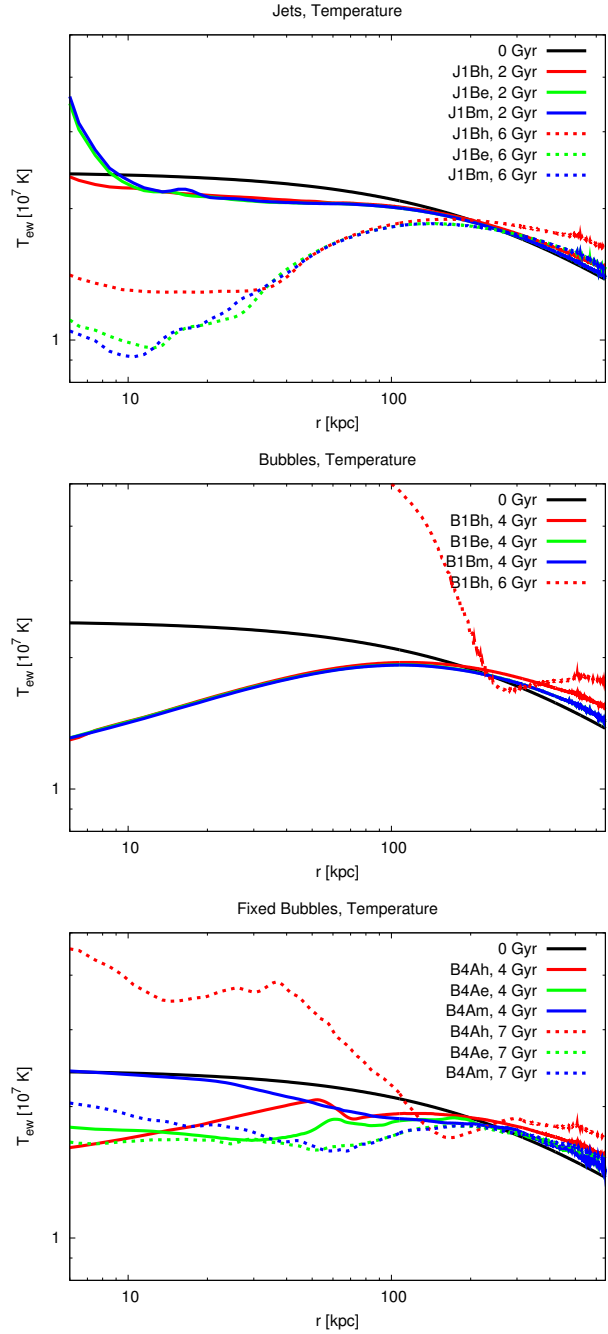


Figure 5. Effects of magnetic injection on the cluster temperature profile. Shown is emission-weighted temperature.

strong outflows prevent further strong feedback events and the magnetic fields in the core push outwards into the cluster medium without being replenished. The jets, however, continuously operate and are always able to magnetize the core. Thus while initially the jets provide the weakest magnetic fields in the core they eventually build up enough strength to provide roughly the same magnetization as the fixed bubbles after 6 Gyr. Randomly-placed bubbles are the least efficient at magnetizing the core, since the bubbles are large and off-center. However, they do begin to produce strong fields after 4 Gyr.

Jets and fixed bubbles exhibit similar patterns when

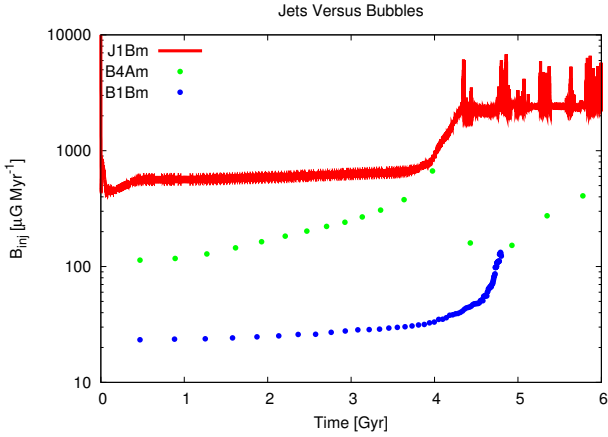


Figure 6. Rate of injected magnetic field strength. Shown is B_{inj} versus time for models J1B, B4A, and B1B. The continuous injection rate for J1B is shown as a line while the points represent the discrete injection events for models B4A and B1B.

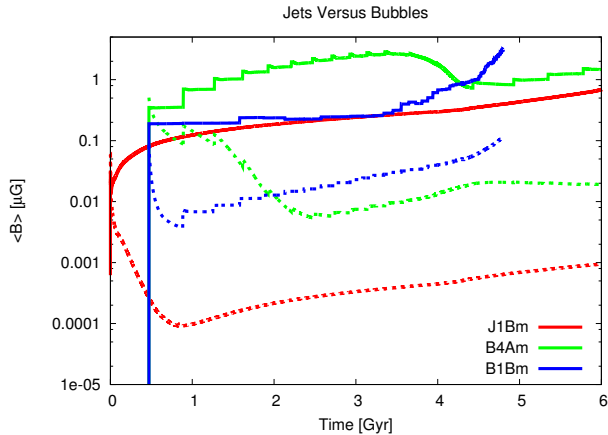


Figure 7. Average magnetic field strength with jets and bubbles. Solid lines are density-weighted average fields within R_{core} and dotted lines are volume-weighted fields within R_{200} .

averaging fields over the entire cluster. Here the initially-injected fields quickly disperse throughout the intracluster medium but eventually weaken by escaping beyond R_{200} via adiabatic expansion and through numerical diffusion. However, fields from the core eventually make their way to the outer regions of the cluster and after 1-2 Gyr the average fields begin to rise again. The bubbles maintain cluster-wide fields over an order of magnitude stronger than the jets, mainly because the bubbles inject their fields farther out from the core, allowing them to more easily propagate into the cluster. The large bubbles of the randomly-placed bubble model eventually provide magnetic fields throughout the cluster as strong as the fixed bubbles.

Next we can study the growth rate of magnetic fields within the cluster volume in Figure 8. Here we show the total volume encompassed by fields of strength at least 10^{-12} G and 10^{-6} G. While all models are able to weakly magnetize the entire cluster, they differ substantially in the time taken to do so. The jets (model J1B) continuously inject strong fields in the core which push out weaker fields into the

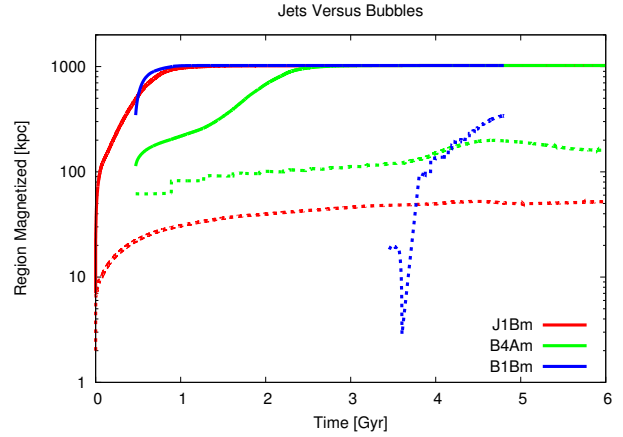


Figure 8. Volume magnetized due to jets and bubbles. Shown is the cube root of the total volume containing fields of strength at least 10^{-12} G (solid lines) and 10^{-6} G (dotted lines).

cluster, saturating the cluster within 1 Gyr. The randomly-placed bubbles (model B1B) saturate the cluster almost immediately since the bubbles are very large and centered away from the core. The fixed bubbles (model B4A) take the longest, 2 Gyr, since these injected fields are centered at the core but are much weaker than the fields injected by the jets and hence less efficient at pushing weaker fields throughout the cluster.

Strong fields permeate a much smaller volume, with jets only able to provide $\sim \mu\text{G}$ fields within the inner 50 kpc. The fixed bubbles, with radii of 40 kpc, are naturally able to strongly magnetize almost the entire core out to a radius of 100 kpc and maintain this magnetization for five billion years. The randomly-placed bubbles cannot produce significant magnetic fields until multiple bubbles overlap so that their magnetic contributions can add together, which does not occur until 3.5 Gyr of evolution. These fields quickly disperse but recover when the bubble feedback becomes strong enough to continuously produce strong fields.

Figure 9 shows the total kinetic and magnetic energies within the entire cluster volume as a function of time. The evolution of the magnetic energy follows the same evolution as the injection rate. The kinetic energy follows a strongly periodic behavior as gas cools and accretes onto the black hole and is driven outwards by outflows. The kinetic energy for all cases also follows the magnetic energy, since magnetic tension in the injected fields drives additional gas motions. Since the fields of the jet model are centrally located, they are less likely to drive large-scale complicated gas motions, whereas the bubbles with large, diffuse, tangled magnetic fields generate complicated gas motions. The turbulence due to these bubbles produces kinetic energies an order of magnitude larger than that due to the jets.

Finally we show radial profiles of the magnetic field in Figure 10 at 3 and 6 Gyr. We construct these profiles from volume-weighted averaging of the field in 1 kpc shells. At 3 Gyr, the fixed bubbles maintain the strongest fields (10 times stronger than the jets and 30 times stronger than the randomly-placed bubbles) within the central 100 kpc but at large radii these fields diminish rapidly. Both bubble models have the same profile shape: an inner plateau

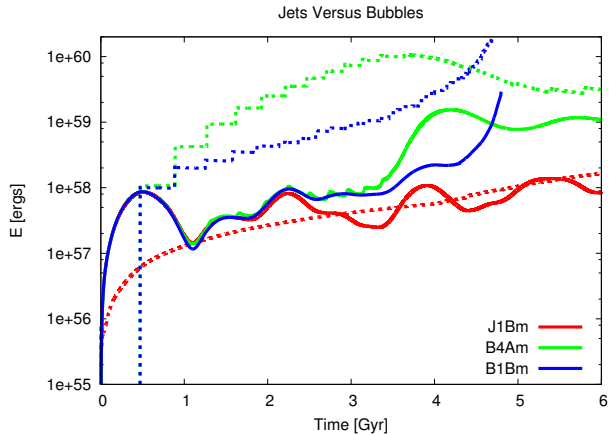


Figure 9. Total cluster kinetic and magnetic energy versus time. Solid lines are kinetic and dotted lines are magnetic energy.

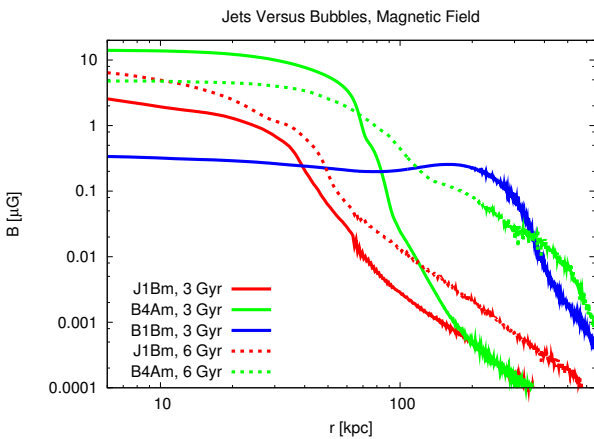


Figure 10. Volume-weighted magnetic field as a function of radius.

where the fields are injected and a steep reduction in field strength beyond that radius. The randomly-placed bubbles, which place weaker magnetic fields within a larger region, maintains this plateau to almost 300 kpc, which is sensible because the bubbles involved have typical radii of 150 kpc. The jets produce a gradually declining field within the inner 50 kpc and the strongest fields in the innermost core, as expected. All the models produce only weak fields ($< 10^{-12}$ G) beyond a radius of 600 kpc.

At 6 Gyr, both the jets and fixed bubbles (the randomly-placed bubbles only evolved to 4 Gyr) exhibit opposite trends. The jets continuously amplify the fields in the core, boosting the field strength in the inner 50 kpc by a factor of four while continuing to strengthen the magnetic fields at larger radii. The fixed bubbles, however, experience a drop in accretion rate at ~ 4 Gyr and hence their ability to magnetize the core after that diminishes. Thus the fields from the inner regions of the cluster just propagate outwards, magnetizing the remainder of the cluster while reducing the magnetization of the core. After 6 Gyr the jets eventually produce the strongest magnetic fields in the core, but the fixed bubbles generate a more highly-magnetized cluster overall.

6 MAGNETIC FIELD TOPOLOGY

We now turn to the topology of the fields produced by our fiducial jet and bubble models: J1B to represent the jets, B1B for randomly-placed bubbles, and B4A for fixed bubbles. Field lines demonstrate the complex morphology produced by the AGN-based injection. We generate field lines by seeding 100 tracer particles uniformly on a sphere of radius 300 kpc. Figure 11 shows the field lines for the fiducial models at various times. Each model is shown at 1 and 3 Gyr and at a time just before complex fields prevent further calculation. Thus we show the field lines at 6 Gyr for the jets, 4 Gyr for the randomly-placed bubbles, and 8 Gyr for the fixed bubbles.

The jets initially produce a toroidal shape with a very regular structure: as the fields are injected as a torus they push out already-present fields which maintain their structure. After 3 Gyr the fields elongate along the jet axis forming a tower with cavities opening in the plane perpendicular to the jet. The magnetic field is able to escape quickly along the jet axis, quickly magnetizing volumes outside the core. Finally, at 6 Gyr, the gas is able to cool sufficiently to begin accreting, dragging the field lines along with it as it accretes onto the core. We thus form a dense cocoon of magnetic field lines. These fields are only slightly tangled and maintain their regular torus-like structure, though stronger fields have been able to propagate farther into the cluster.

The randomly-placed bubbles exhibit complex, tangled behavior almost immediately. While each bubble contains a torus-like magnetic field, as multiple bubbles form and overlap the fields entangle. The bubbles are able to form strong fields with complex structures far from the central core. At later times more bubbles form and overlap, increasing the average magnetic field in the core. Few magnetic field lines are able to escape into the outer cluster regions, even after 4 Gyr. However, the volume magnetized by bubbles is much larger than that of the jets. The bubbles are also much more asymmetric than the fields produced by the jets, since each injected bubble has a new, random field orientation.

The fixed bubbles initially exhibit only somewhat ordered topology. While each bubble has the same magnetic field orientation, between bubble events some magnetic field lines can escape and turbulence caused by the infalling gas can twist and tangle the fields. At 3 Gyr, however, the bubbles appear frequently enough to maintain a torus-like topology. Eventually the fields collapse due to the asymmetric infill of the gas, and a large parcel of magnetic field lines escapes along the jet axis, leading to a complex topology containing both ordered torus-like and tangled components.

We also show the equipartition case for each fiducial model in Figure 12 at the latest time available for each model. For each model the magnetic fields are weaker than in the purely magnetic case, but the larger topology remains unaffected. The final cocoon created by the jets is smaller since the injected fields are not as strong. The weaker fields of both the randomly-placed and fixed bubbles produce much more disperse field lines. Thus while we affect the overall strength of magnetic fields we do not change the topological structure of the fields when considering injection modes with less magnetic energy. Also, the addition of thermal energy in the equipartition case does not affect the topology of the fields.

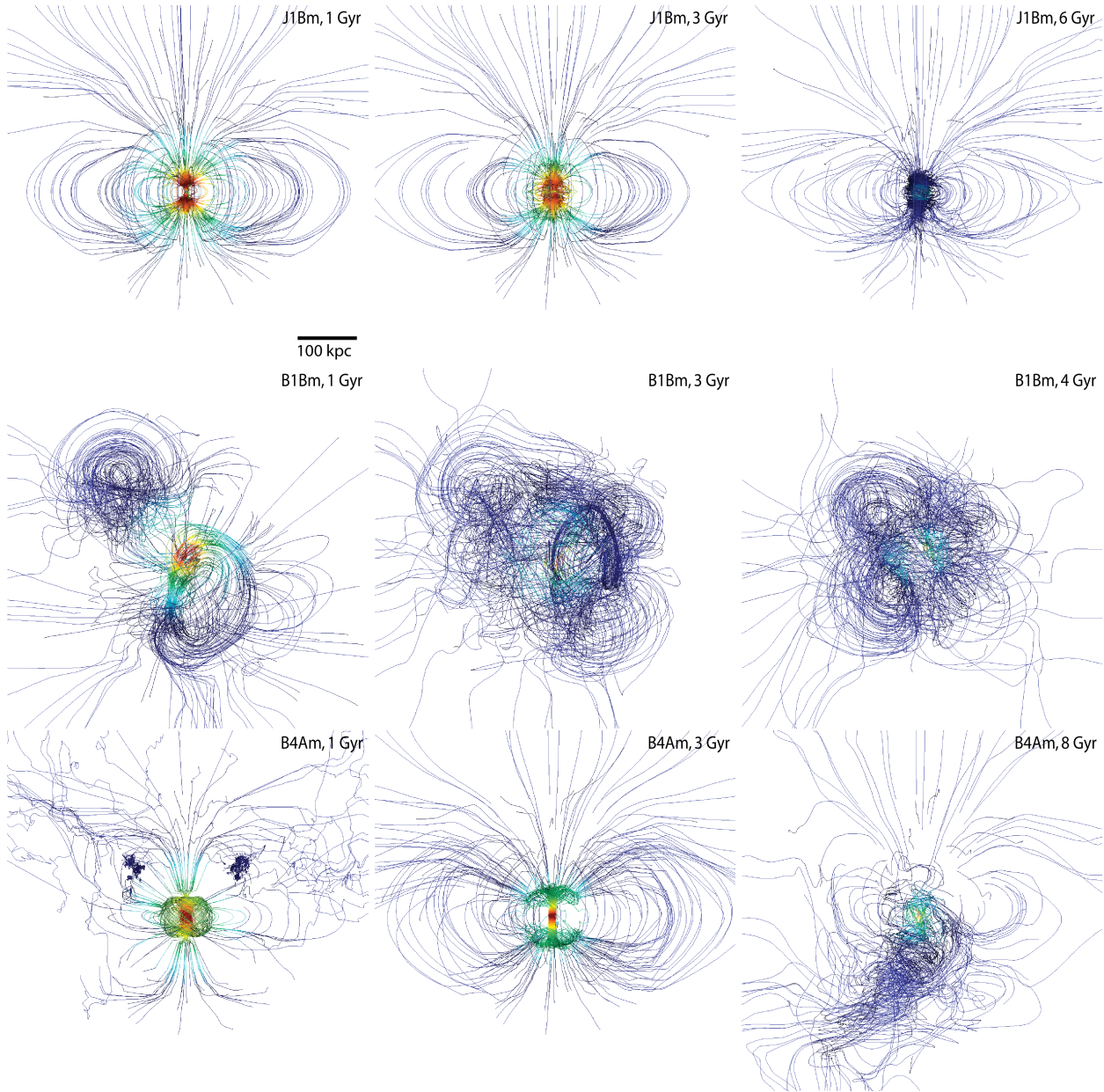


Figure 11. Evolution of magnetic field lines for the fiducial models. Shown are models J1Bm (top), B1Bm (middle), and B4Am (bottom). From left to right, model J1Bm is shown at times 1, 3, and 6 Gyr, model B1Bm is shown at times 1, 3, and 4 Gyr, and model B4Am is shown at times 1, 3, and 8 Gyr. All field lines are constructed using 100 tracer particles uniformly distributed on a sphere with radius 300 kpc. The field lines are colored using the local gas density, with blue colors indicating low density and red colors denoting high-density regions. The view is roughly 600 kpc across.

Next in Figure 13 we see the evolution of the magnetic field in terms of the rotation measure (RM) taken along the x -axis. The rotation measure is defined as

$$\text{RM} = 812 \int_0^L n_e \mathbf{B} \cdot d\mathbf{l} \text{ radians m}^{-2}, \quad (12)$$

where \mathbf{B} is the magnetic field in μG , n_e is the electron density, and \mathbf{l} is the direction of light propagation in kpc (positive values indicate fields pointed towards the observer). The maps shown have a spatial resolution of 4 kpc. In our plots, we have truncated the color scale to indicate RM values between -500 and 500 rad m^{-2} so that we may

readily compare the structures of different injection models. The true minima and maxima for each model are listed in Table 8.

The jets at 1 Gyr show high rotation measure values with very little spatial extent: only ~ 10 kpc perpendicular to the jet and ~ 50 kpc along the jet axis. The RM exhibits the handedness given to the injected magnetic fields, with a value of 150 rad m^{-2} to the left of the jet and -150 rad m^{-2} to the right. At 4 Gyr the strong RM region in the center is slightly larger with peak values about three times stronger. By 6 Gyr the strong feedback episodes have dramatically increased the peak RM value to over 2500 rad m^{-2} and the

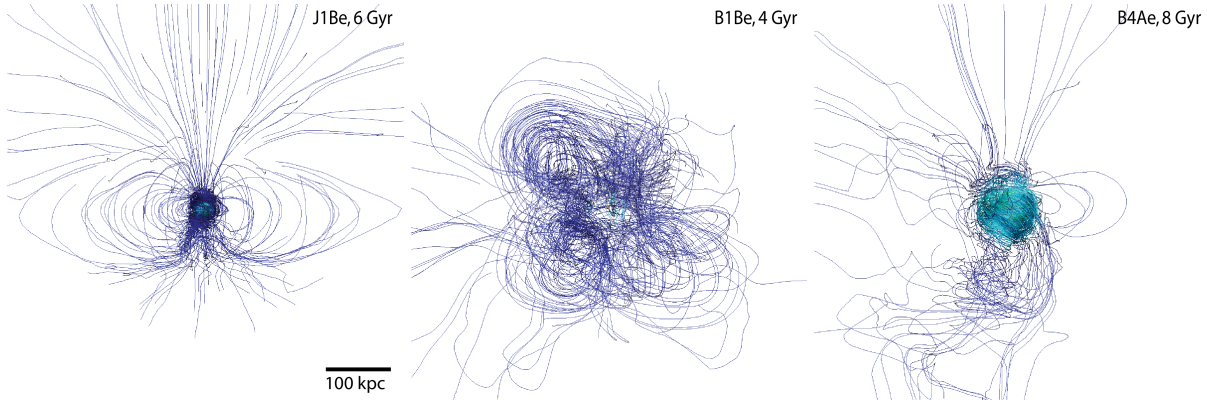


Figure 12. Magnetic field lines from the equipartition injection mode. Shown are models J1Be at 6 Gyr (top), B1Be at 4 Gyr (middle), and B4Ae at 8 Gyr (bottom). Construction of the lines and coloring is identical to Figure 11.

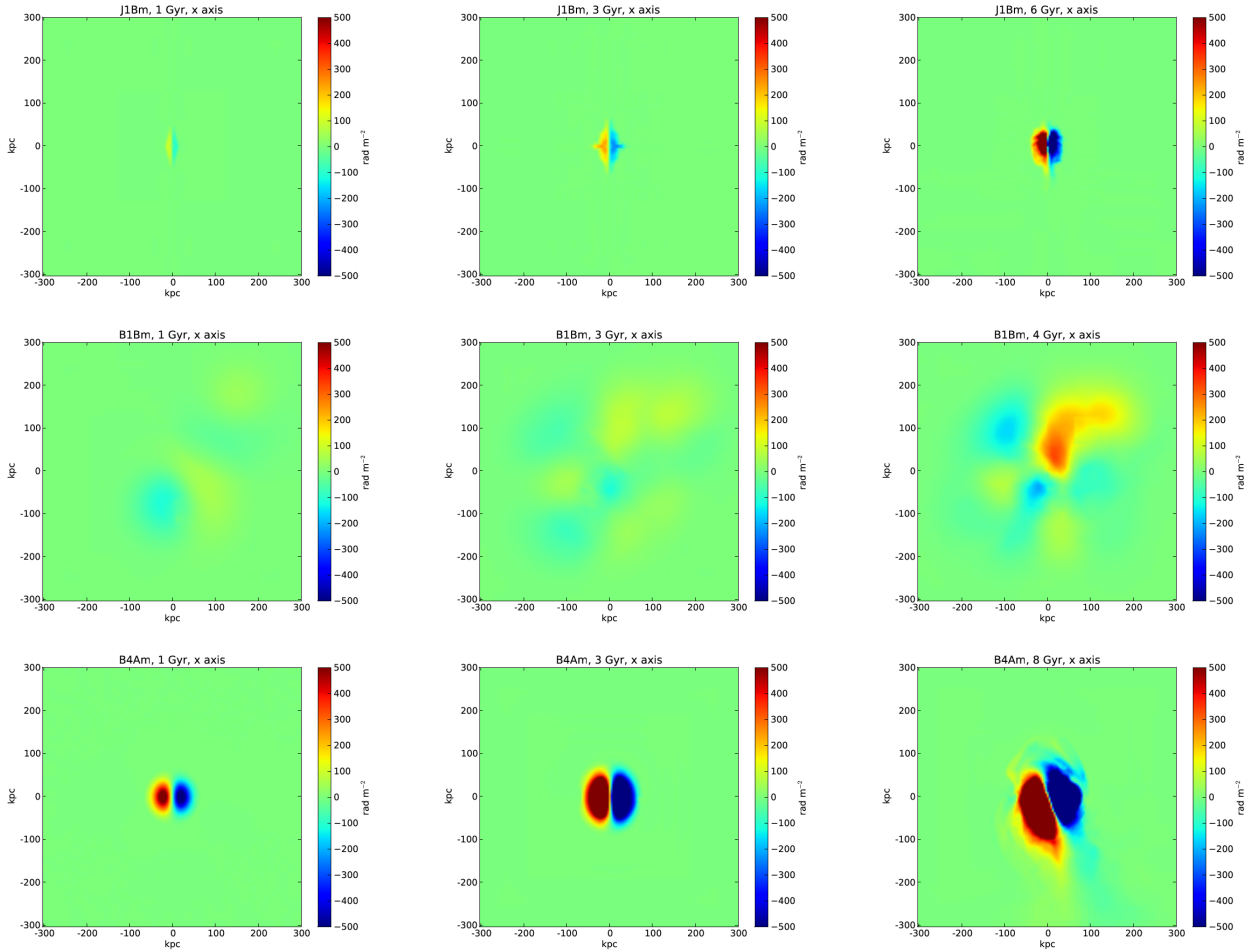


Figure 13. Evolution of the rotation measure for the fiducial models. Shown are models J1Bm (top), B1Bm (middle), and B4Am (bottom). From left to right, model J1Bm is shown at times 1, 3, and 6 Gyr, model B1Bm is shown at times 1, 3, and 4 Gyr, and model B4Am is shown at times 1, 3, and 8 Gyr. All rotation measures are taken along the x -axis and have a uniform resolution of 4 kpc. Note that the color scale is chosen to enhance the regions outside the core. The true minima and maxima for each model are listed in Table 8.

Table 8. Extreme rotation measure values.

Model	Time (Gyr)	Axis	Min	Max
fJ1Bm	6	x	-2132.38	2050.55
fJ1Bm	6	y	-2588.3	1847.2
fJ1Bm	6	z	-437.649	4016.64
fJ1Be	6	x	-1547.93	1695.04
fB1Bm	4	x	-209.177	338.916
fB1Bm	4	y	-244.671	275.929
fB1Bm	4	z	-561.889	115.311
fB1Be	4	x	-150.565	444.04
fB4Am	8	x	-2400.3	3101.37
fB4Am	8	y	-3483.68	1906.73
fB4Am	8	z	-1227.99	7642.16
fB4Ae	8	x	-2448.87	3706.81

collapsing gas has shrunk the volume enclosed by strong magnetic fields. Also, turbulent gas motions have begun to introduce some asymmetry in the RM map; however, the overall structure remains intact.

The magnetic fields produced by the randomly-placed bubbles result in large-scale (~ 400 kpc) weak RM structures within 1 Gyr. However, the RM here is much weaker - reaching a value of no more than 400 rad m^{-2} by 4 Gyr - than those generated by the jets since the magnetic fields are distributed over a much larger volume. As more bubbles form, the peak RM values increase and distribute over a large volume, eventually forming ~ 100 kpc structures surrounding the central core. The fixed bubbles show a similar handedness as the jets since once again each injection is given the same axis. However, the RM here reaches a peak value much stronger than both the randomly-placed bubbles and the jets. Additionally, strong RM values are distributed over a much larger volume, reaching ~ 100 kpc into the cluster atmosphere.

We additionally view the latest times available for each model in the y and z directions in Figure 14. The highly-directional jets show identical RM distributions in both the x - and y -directions, but the rotation measure along the jet axis shows little spatial variation and a very high value within the central 10 kpc. The randomly-placed bubbles exhibit nearly identical morphology along the other axes, as expected by the random orientations given to each injected bubble. The fixed bubbles have similar features to the jets, with large RM values along the z -axis, but with some discernible rotation measure extending out to ~ 100 kpc, much farther than for the smaller jets.

Finally, we can compare equipartition modes to fully magnetized injection with Figure 15. Once again we see little difference in the overall structure for the jets and both bubble models. The values of the peak rotation measures are only slightly less in the equipartition cases than they are in their fully magnetic counterparts. Additionally, the randomly-placed bubbles show a much more smooth and uniform distribution with equipartition injection. The jets and fixed bubbles maintain their spatial extent. Thus we once again see that merely the presence of magnetic injection has significant effects, and that the relative proportion of magnetic to thermal energy is less important.

7 MODEL PARAMETER SURVEY

7.1 Jets

Our jet model parameter survey includes variations in the underlying peak grid resolution, the size of the jet, the value of the accretion strength parameter α , and the size of the accretion and depletion regions. For the plots in this section, we will label the model groups as follows: models J1A-J1C are labeled as “Jet Resolution”, models J2A-J2C are the “Jet Size” group, “Jet Accretion Strength” will refer to models J3A-J3C, and finally models J4A-J4C will be referenced by “Jet Depletion and Accretion”.

These parameter changes significantly affect the accretion history of the SMBH, as shown in Figure 16. With higher resolution (model J1A) the accretion history is much more variable, but the average accretion rate is roughly equal to the fiducial case. In this case the strong injected fields make continuation of the simulation very difficult past 1.5 Gyr, and at this point the combination of turbulent gas motions and strong fields make the accretion rate highly variable. When we vary the jet size we get more diverse behavior and longer-lasting jets. In model J2A, where we double the size of the jets, we maintain the same average accretion strength as in the fiducial case but add the periodic behavior seen with the well-resolved jets of model J1A. As we increase the jet size while fixing $\Delta x = 1.0$ kpc in models J2B and J2C we see a consistent increase in the average accretion rate. As the jet energy gets deposited in a larger volume the magnetic fields become less effective at keeping gas away from the central black hole. When we decrease the relative size of the jet in model J2D, the smaller jet becomes more effective at removing gas, thereby lowering the accretion rate relative to the J2C model, which has the same resolution but a larger jet.

When we vary the accretion strength parameter α (models J3A-C), we see similar evolution patterns in the accretion rate, though the rates are uniformly higher than the fiducial case. Model J3A, which both lowers the resolution to $\Delta x = 0.5$ kpc and raises α to 100, produces incredibly strong fields within 0.5 Gyr, preventing further simulation. However, prior to this point there still appears to be some periodicity with features similar to model J1A, which has the same resolution but $\alpha = 1$. Interestingly, setting $\alpha = 100$ does not produce an accretion rate that is 100 times higher. Instead, the stronger outflows are more effective at pushing away gas from the core, lowering the overall accretion rate to just a factor of five larger than the fiducial case. Similarly, with $\alpha = 300$ in model J3C we do not see a corresponding tripling of the accretion rate.

Varying the depletion and accretion radii can have some significant effects, especially if these values are larger than the injection region. Model J4A sets $R_{\text{dep}} = R_{\text{acc}} = \Delta x$ (i.e., one zone), and we do not see significant differences between this and the fiducial case. This is also the case when we remove depletion altogether, as in model J4C. Since the accretion rate is incredibly small for the jets in the first place, removing gas has no significant effects. However, when we set the accretion and depletion radii to 4 zones, as in model J4B, we see an initially larger accretion rate followed by a factor of five jump after only 1 Gyr, rather than the 4 Gyr it takes in the fiducial model. In this case, we are measuring within a volume slightly larger than the injection region

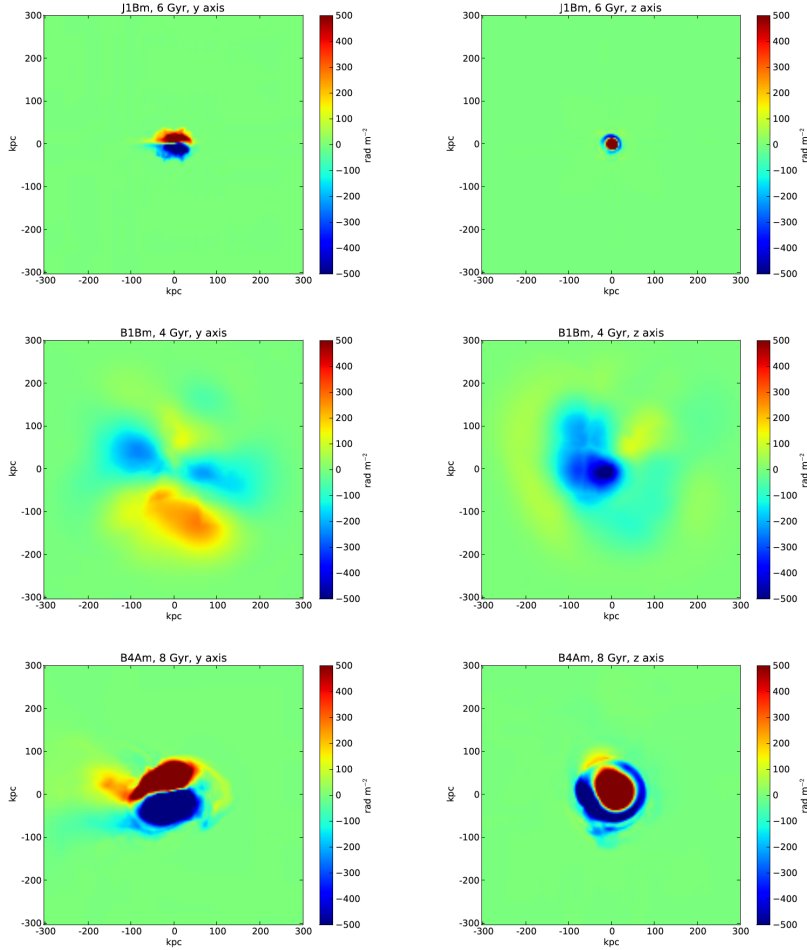


Figure 14. Rotation measure taken along the y -axis (left) and z -axis (right). Shown are models J1Bm at 6 Gyr (top), B1Bm at 4 Gyr (middle), and B4Am at 8 Gyr (bottom). All rotation measures have a uniform resolution of 4 kpc. Note that the color scale is chosen to enhance the regions outside the core. The true minima and maxima for each model are listed in Table 8.

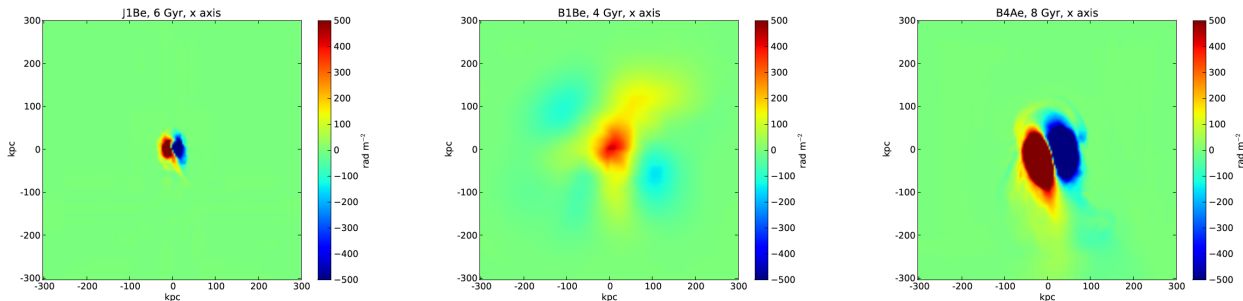


Figure 15. Rotation measure from the equipartition injection mode. Shown are models J1Be at 6 Gyr (left), B1Be at 4 Gyr (middle), and B4Ae at 8 Gyr (right). All rotation measures are taken along the x -axis and have a uniform resolution of 4 kpc. Note that the color scale is chosen to enhance the regions outside the core. The true minima and maxima for each model are listed in Table 8.

itself (note that the injected magnetic fields are strongest at the scaling radius, which is one half the injection radius) and the gas that the magnetic fields drive away from the core gets included in the accretion rate calculation, leading to an increase in the accretion rate. Also the large jump in accretion rate occurs earlier since we are measuring at a larger radius, and the cooled gas does not take as long to

reach the inner 4 kpc as it does to reach the inner 2 kpc, where the magnetic injection is strongest.

In Figure 17 we see how varying the jet parameters affects the rate of injected magnetic field strength. For model J1A, despite the small changes to the accretion rate, the injected magnetic field rate is almost a factor of two higher. This is mainly due to a severely decreased time step in the

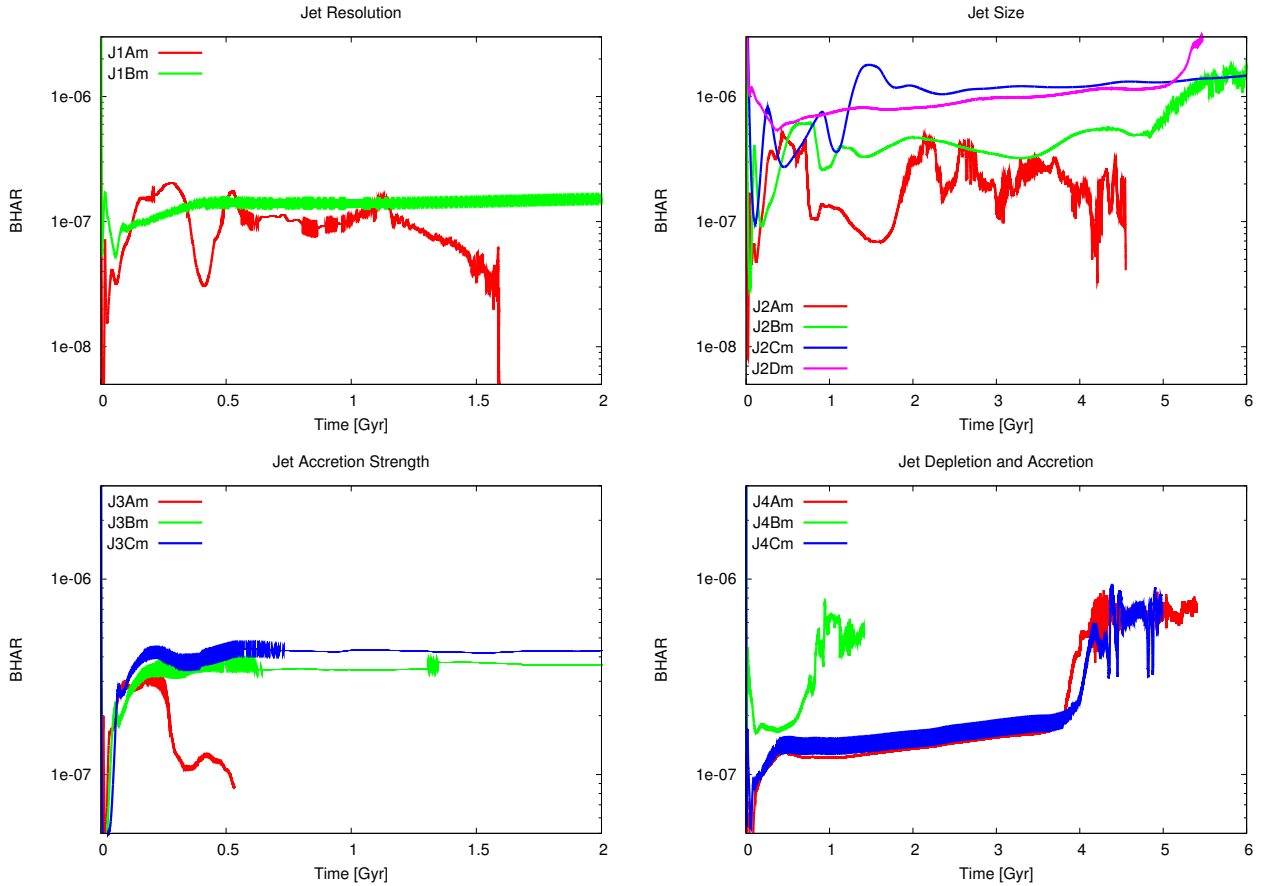


Figure 16. Affecting the black hole accretion rate by varying the jet model parameters. Shown is BHAR ($\dot{M}/\dot{M}_{\text{Edd}}$) versus time.

J1A run: although the instantaneous accretion rate, and hence the injected magnetic energy, may be lower, the total injected magnetic field over long periods of time is larger in the higher-resolution run. When we vary the jet size, we find that model J2A, despite having the lowest accretion rate, has the highest rate of injection of magnetic fields. This is because this model injects magnetic fields into the smallest region. The resulting field is more strongly concentrated, leading to a higher B . As we scale to ever-larger jets, the fields are distributed over larger volumes, and hence the B_{inj} rate drops. Model J2D, which has a lower resolution but same jet size as J2B, maintains roughly the same injection rate, consistent with the view that lower resolutions do not significantly alter the resulting magnetic fields.

Varying the accretion strength parameter α has almost no effect: since the accretion rate self-regulates with changes in α , models J3B and J3C are not significantly different. However, model J3C, with a larger α of 300, does produce slightly stronger magnetic fields. When we vary the accretion and depletion radii, we once again see only strong differences with model J4B, which produced fields almost an order of magnitude stronger than the fiducial case after only 1 Gyr.

Figure 18 shows the changes to the average magnetic field strength within R_{core} and R_{200} . The higher-resolution jets (J1A) and large jets (J2C) are best at magnetizing both the inner and outer cluster regions. As expected, the large jets are able to distribute fields over a much larger volume

than the fiducial case, although they cannot produce fields stronger than $\sim 1 \mu\text{G}$ in the core. There is again no significant difference when increasing α from 100 to 300, although these models produce slightly stronger fields within the core compared to the fiducial case. Despite the enhanced accretion rate of model J4B, we do not evolve the jet long enough to see significant differences in the average field of the core. However, we do begin to see an increase in the overall magnetization of the cluster, with roughly a doubling of the average cluster-wide field.

We see similar trends in the magnetized volume, as shown in Figure 19. The large jets and high- α jets push weak magnetic fields throughout the cluster volumes in less than 500 Myr, whereas the fiducial case takes almost twice as long. However, the high- α models still do not push strong fields very far into the cluster - only to ~ 50 kpc. On the other hand, the large jets can generate strong fields out to 100 kpc. Also, here the effects of higher resolution are less pronounced. With the boosted accretion rate of model J4B, the cluster saturates with weak magnetic fields much more quickly (less than half the time of the fiducial case), with a slight increase in the volume of strong magnetic fields. Once again, we do not see large differences with the smaller accretion and depletion radii relative to the fiducial model.

Finally, we see in Figure 20 the radial profiles of the magnetic fields. We first see that model J1A, which has higher resolution than the fiducial case, is able to provide

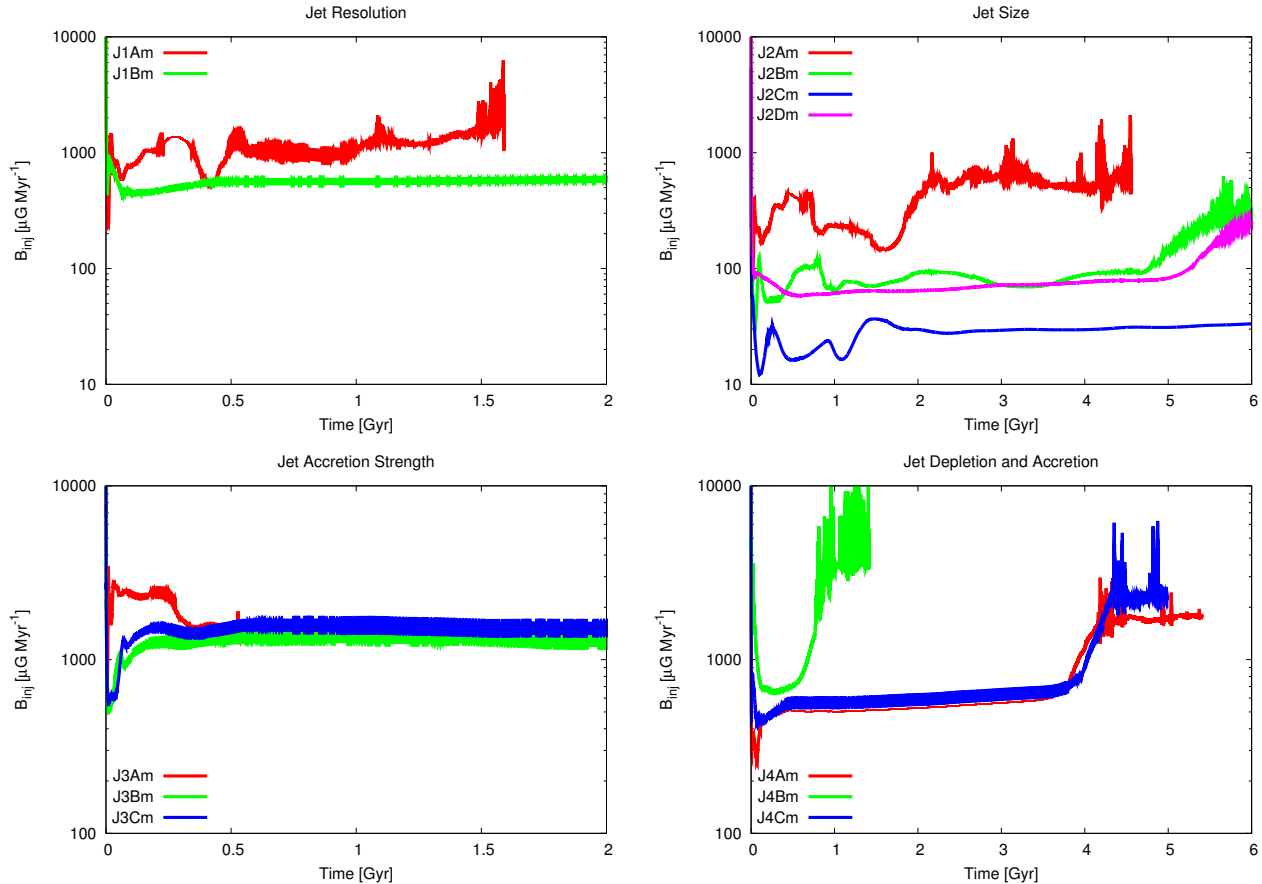


Figure 17. Affecting the rate of injected magnetic field strength by varying the jet model parameters.

more magnetization throughout the cluster in 1 Gyr than the fiducial case is able to produce in twice that time. All of the large jets are able to generate strong fields in the core (over $10 \mu\text{G}$ in some case) after 6 Gyr. However, since the magnetic fields of model J2C are distributed over such a large volume, the strongest fields in the core come from the slightly smaller jets of model J2B. When we increase α in models J3B and J3C, we see almost no differences in the profiles at 1 and 2 Gyr. Also, there is very little difference between either of these models and the fiducial case. Model J4B, with the larger accretion and depletion radii, produces an order of magnitude stronger field at large radii and nearly a doubling of the field in the inner cluster after only 1 Gyr.

7.2 Bubbles

By varying the peak resolution and accretion strength in the bubble models we also see significant differences in the accretion rate, magnetic outflow properties, and overall magnetization of the cluster. The plots in this section are split into two groups: “Bubble Resolution” will contain models B1A–B2E, and “Bubble Accretion Strength” will reference models B2A, B2B, B3A, and B3B.

Our parameter changes significantly affect the accretion rate, as shown in Figure 21. First, changing the resolution has a stronger effect on the bubbles than the jets, mostly because we can reduce the resolution much further than in

the jet models and still adequately resolve the bubbles. At the same resolution as the jets (0.5–1.0 kpc) we see very little difference. However, at lower resolutions (4–8 kpc), we begin to see much lower accretion rates as time progresses, reaching an order of magnitude in difference at 5 Gyr. At lower resolutions, we also delay the onset of the formation of highly complex fields by over a billion years, so the simulations can evolve further.

When we vary the accretion strength parameter α , we see much more complicated behavior than in the jets. Whereas the jets maintained self-regulated behavior, because the continuous jet-based feedback was coupled more tightly to the immediate surroundings of the black hole, the bubbles are much more sensitive to changes in α . As we increase α , as in models B2A and B2B, we see immediate increases in the BHAR. The bubbles, which take time to form and are not as efficient as the jets at driving gas away from the core, only slightly reduce the accretion rate below the amplified value. For example, setting $\alpha = 100$ produces a BHAR only ~ 80 times stronger rather than 100. As we vary the resolution along with α , as in models B3A and B3B, we see that the changes to the accretion strength are dominant over the changes to resolution.

The bubble sizes vary dramatically, as shown in Figure 22. Note that as we lower the resolution (and have correspondingly lower accretion rates) our bubbles become slightly *larger*. Since the bubble energy is fixed as a frac-

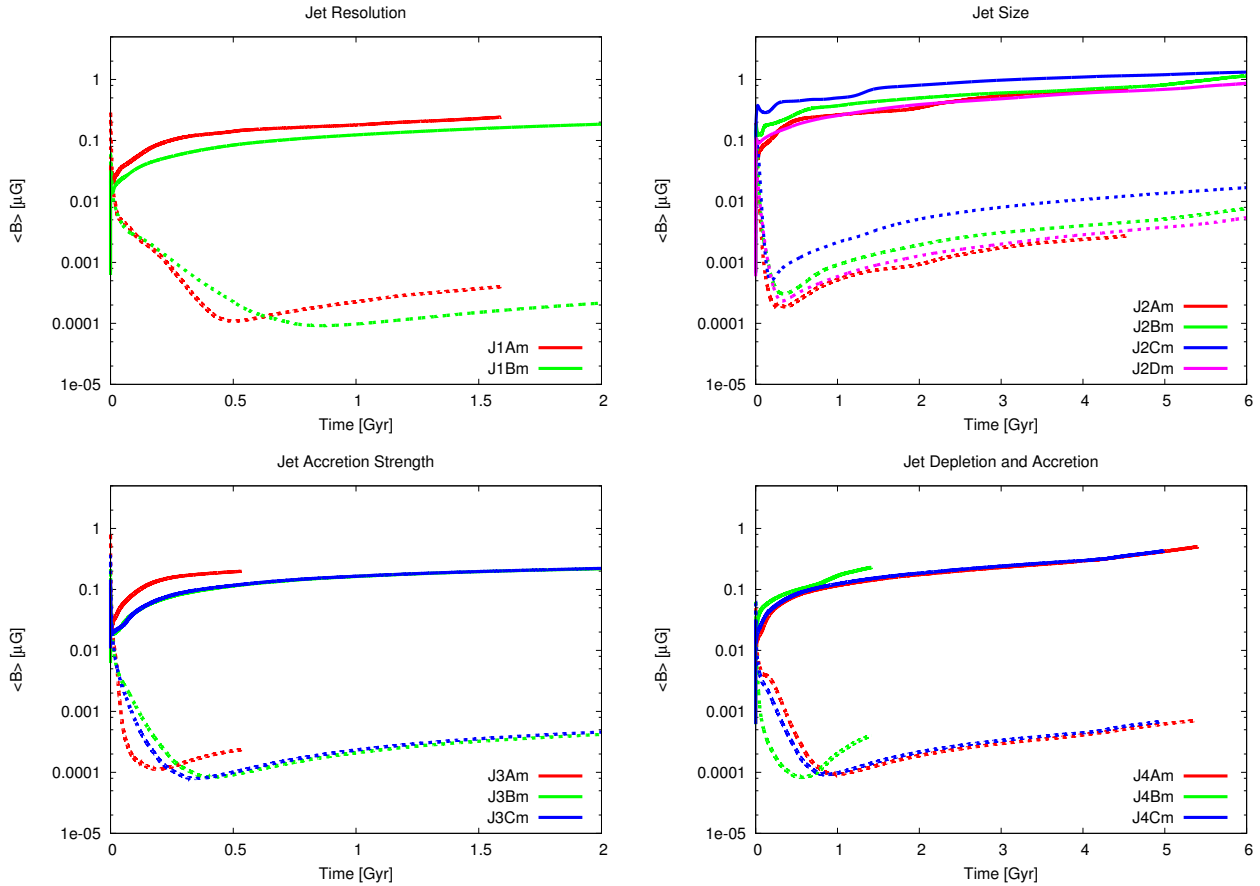


Figure 18. Affecting the average magnetic field strength by varying the jet model parameters. Solid lines are density-weighted average fields within R_{core} and dotted lines are volume-weighted fields within R_{200} .

tional increase in the SMBH mass, at lower resolutions we begin to underestimate the gas density, which both lowers the accretion rate and produces larger bubbles, as Eq. 7 suggests. Notice that it also takes longer to produce bubbles at lower resolutions, taking almost twice as long in the 8 kpc case than in the 4 kpc run.

Authors usually invoke an enhanced accretion strength parameter to account for underestimating the gas density at lower resolutions. However, for this cluster our changes to α dominate over changes to resolution. Note especially models B3B and B1B. Model B3B has a resolution of 4 kpc, and an α of 300 should account for the resulting under-resolution of the gas density. Instead, model B3B produces many more bubbles with larger radii and begins a periodic cycle within 1 Gyr, which are features absent from model B1B. We also notice some discontinuities, such as in model B3B, where strong bubble events temporarily halt the cooling of gas. All of the runs with increased α produce unphysically-large bubbles (> 200 kpc) with extremely high formation rates (one bubble per 10-20 Myr), suggesting that increasing α may not always be appropriate.

Despite the small changes to the accretion rate and bubble size when changing the resolution, we see dramatic differences in the magnetic injection rate, as shown in Figure 23. Even though the injected energy is the same for each bubble event (Eq. 6), this energy is distributed over different bubble volumes. Hence, small changes in the bubble radius lead

to large differences in the injected magnetic field strength. The smallest bubbles, which occur with $\Delta x = 0.5$ kpc in model B1A, have the largest injected field strength, with a B_{inj} for the first bubble over a factor of two larger than that of model B2A, which has a resolution of 1.0 kpc. The trends continue down to 4 kpc. However, at this resolution the bubbles are already so large that at lower resolutions there is little difference in the injected field strength. For all these models the injection rate steadily increases as gas cools and accretes onto the core, eventually producing magnetic fields which are too strong and tangled (which drives the timestep lower) to simulate further.

With the boosted- α models we again see large differences in B_{inj} . However, instead of the steadily increasing magnetic field strength of the $\alpha = 1$ models, small cyclic variations in the accretion rate and bubble size lead to similar, but amplified, patterns in the rate of injected field strength. This is most evident in model B2B, where the injection rate changes by a factor of ~ 5 with a period of roughly 1 Gyr.

The smaller bubbles in the high-resolution runs are more effective at magnetizing the cluster, as we show in Figure 24. Reduced numerical dissipation as we increase resolution also plays a role; however, the changes in the accretion rate due to resolution, and hence the resulting feedback energy, dominate over any effects of numerical resistivity. This figure displays the average magnetic field strength within

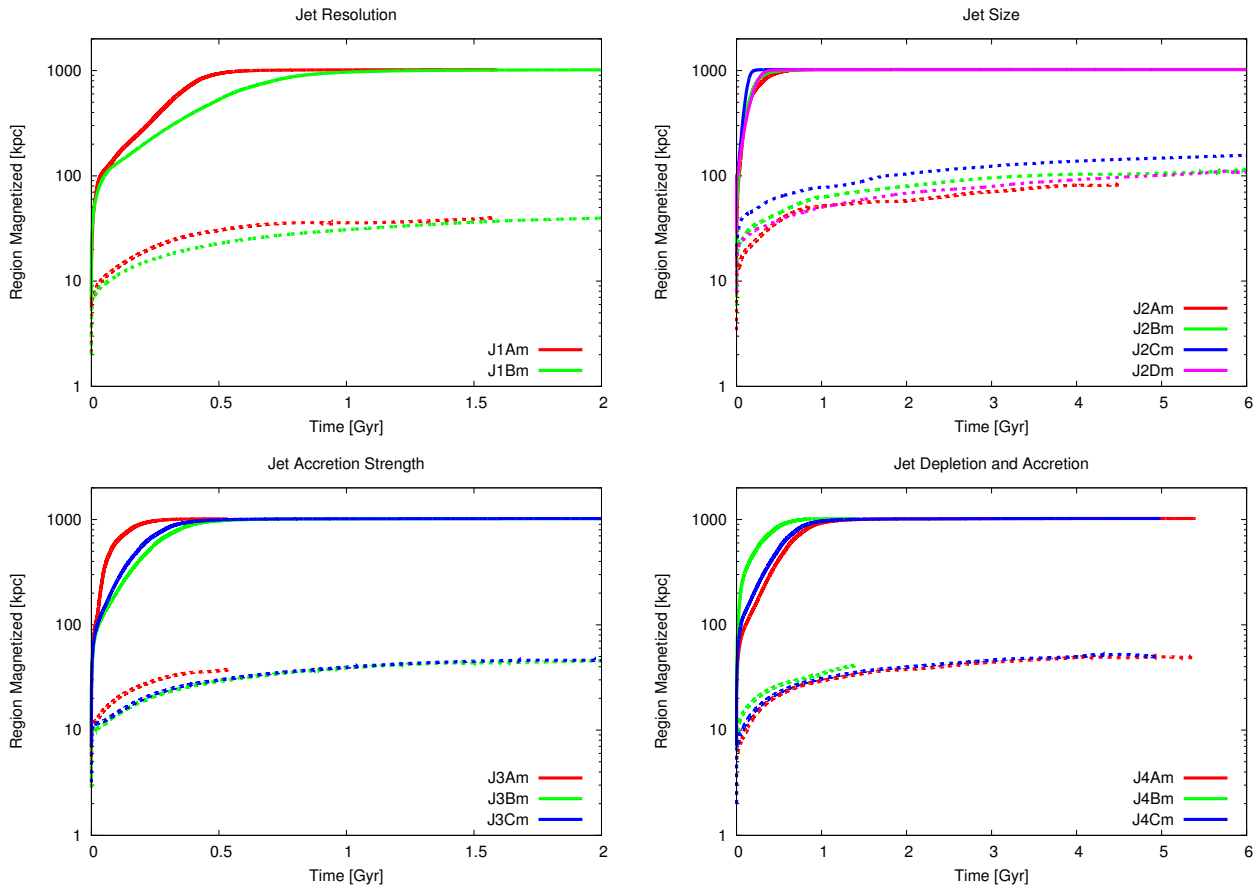


Figure 19. Affecting the volume magnetized by varying the jet model parameters. Shown is the cube root of the total volume containing fields of strength at least 10^{-12} G (solid lines) and 10^{-6} G (dotted lines).

the core and within the entire cluster. Model B1A is able to generate $1 \mu\text{G}$ fields within the core in 3 Gyr, whereas model B1D, with 16 times lower resolution, takes twice as long. All of these models produce the same general trends: steadily-increasing magnetic fields both in the core and entire cluster from 1 to 4 Gyr followed by a sharp rise as the accretion intensifies.

We again see the strong dependence on accretion strength parameter: the high- α runs generate $> 1 \mu\text{G}$ fields within the core and $> 0.1 \mu\text{G}$ fields averaged within the entire cluster in less than 1 Gyr. Indeed, models B2B and B3B, with $\alpha = 300$, are able to produce $\sim 1 \mu\text{G}$ fields within R_{200} . The higher the value of α , independent of resolution, the greater the magnetization. The time-dependent behavior of the average field within the cores for these models looks more like the jets than the fiducial bubble case.

In all bubble cases, regardless of changes to the resolution or accretion strength, the cluster quickly magnetizes, as we see in Figure 25. However, the high- α models not only magnetize the cluster with weak fields, but also push strong ($> 1 \mu\text{G}$) fields almost to the cluster edge. The $\alpha = 1$ cases, however, are much less effective at generating these strong fields, with most models only creating these fields after 3 Gyr. These models are also only able to push these fields to a meager ~ 200 kpc radius.

This is also reflected in the radial profiles of the magnetic fields, which we show in Figure 26. All the high- α

models create a region of strong fields out to ~ 400 kpc within only 1 Gyr. This is due to the strength and frequency of these bubbles. After another 2 Gyr of evolution the fields in this same region have doubled in strength. On the other hand, varying the resolution does not produce significant differences until 5 Gyr of evolution. In all these cases, the fields remain relatively constant out to a radius of 200 kpc before steeply falling, and changes to the resolution do not affect this behavior. While higher resolution does result in stronger fields, a factor of 16 difference in resolution only produces a factor of 2 difference in the resulting magnetic fields, even after billions of years of evolution.

8 DISCUSSION & CONCLUSION

We have conducted a systematic study of the growth and evolution of magnetic fields due to the self-regulated feedback of a central active galactic nuclei within an isolated mock cluster. This study is the first to link the energy available for injected magnetic fields to an accretion rate measured on the simulation mesh. We have implemented magnetic field injection using representative models of continuous small-scale jets and sporadic large-scale bubbles. We have examined the effects of magnetizing the jet and bubble outflows on the accretion properties of the black hole and the thermodynamic quantities of the surrounding clus-

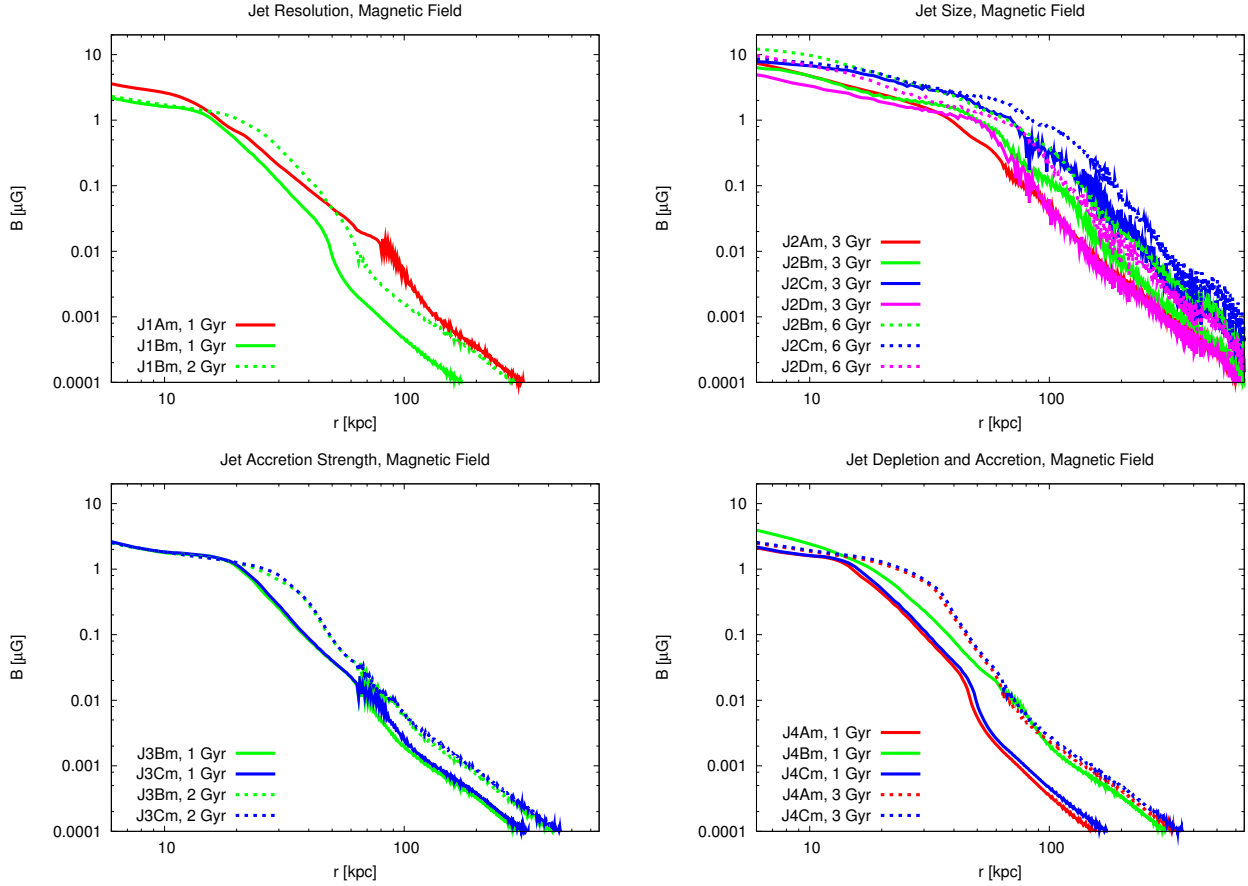


Figure 20. Affecting the magnetic profiles by varying the jet model parameters. Shown are volume-weighted magnetic fields as a function of radius.

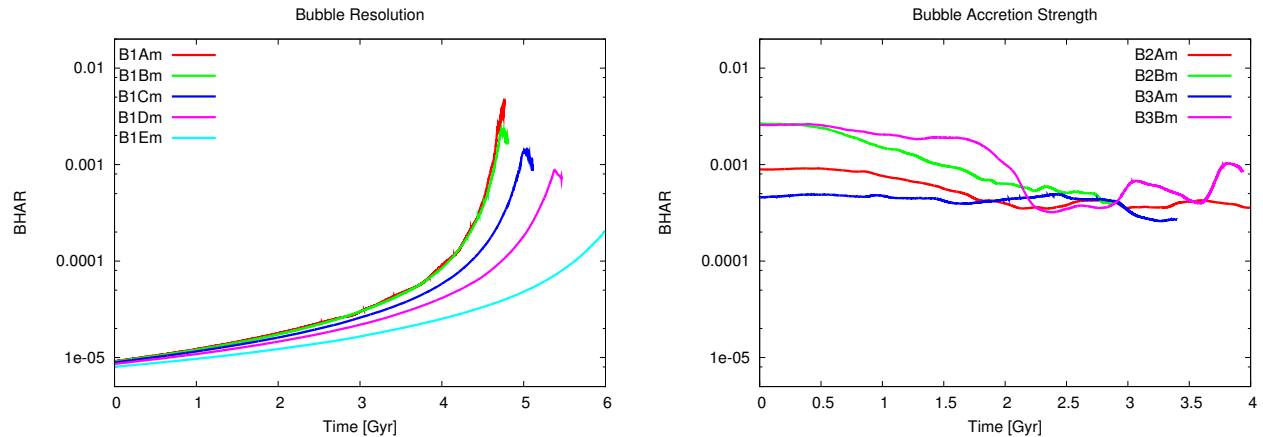


Figure 21. Affecting the black hole accretion rate by varying the bubble model parameters. Shown is BHAR ($\dot{M}/\dot{M}_{\text{Edd}}$) versus time.

ter gas. We have compared the resulting magnetization of the cluster using a fiducial jet and bubble model in terms of the growth, evolution, and topological structure of the magnetic fields. Finally, we have performed a parameter survey of the jet and bubble models to determine the relationship between subgrid model parameter choices and the resulting magnetic outflow properties.

The relative effects of adding magnetic fields into the

injection depend on the choice of subgrid model. Continuous jets, where the feedback is applied to the central few zones, suffer a large decrease in the accretion rate due to the tension forces inherent in the injected magnetic fields. Fixed-position bubbles, with large radii, take roughly 3 Gyr for noticeable differences to emerge, while randomly-placed bubbles are almost entirely unaffected. While it is thought that the evolution of bubbles is dominated by the presence

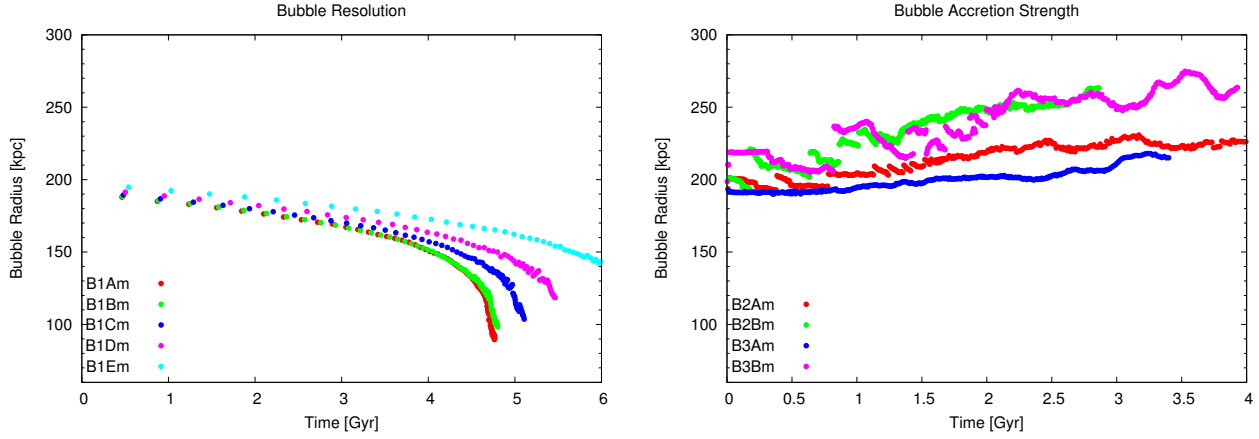


Figure 22. Affecting the bubble size by varying the bubble model parameters. Shown is bubble radius at each injection event as a function of time.

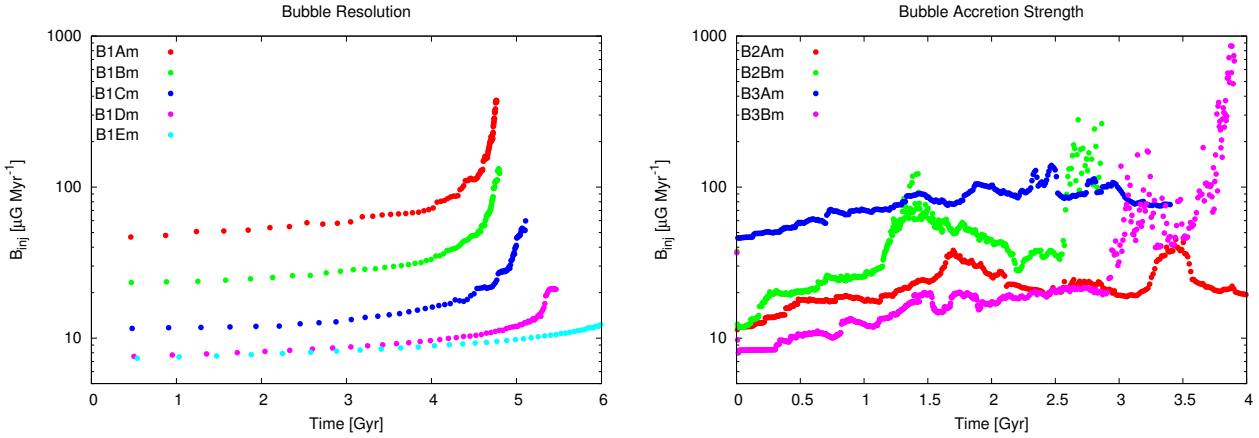


Figure 23. Affecting the rate of injected magnetic field strength by varying the bubble model parameters.

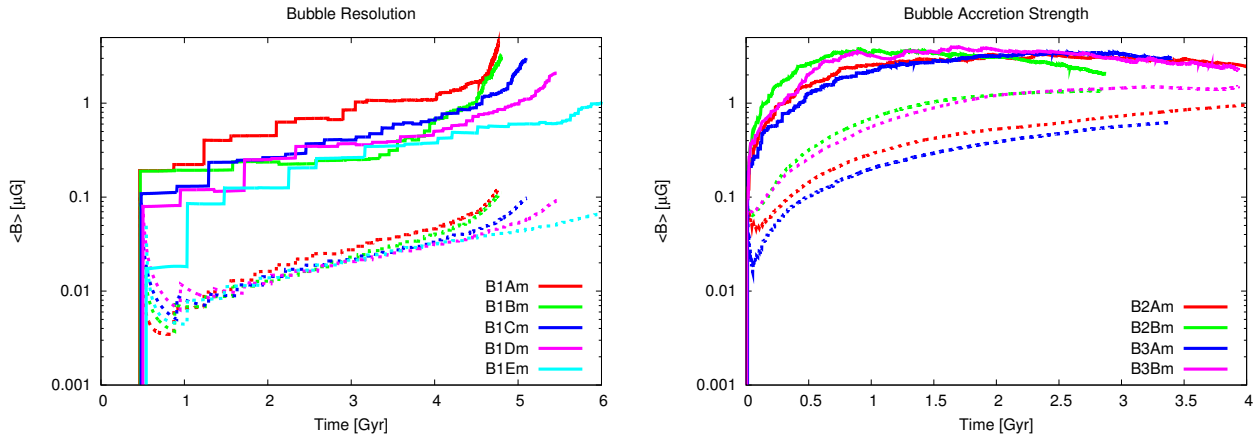


Figure 24. Affecting the average magnetic field strength by varying the bubble model parameters. Solid lines are density-weighted average fields within R_{core} and dotted lines are volume-weighted fields within R_{200} .

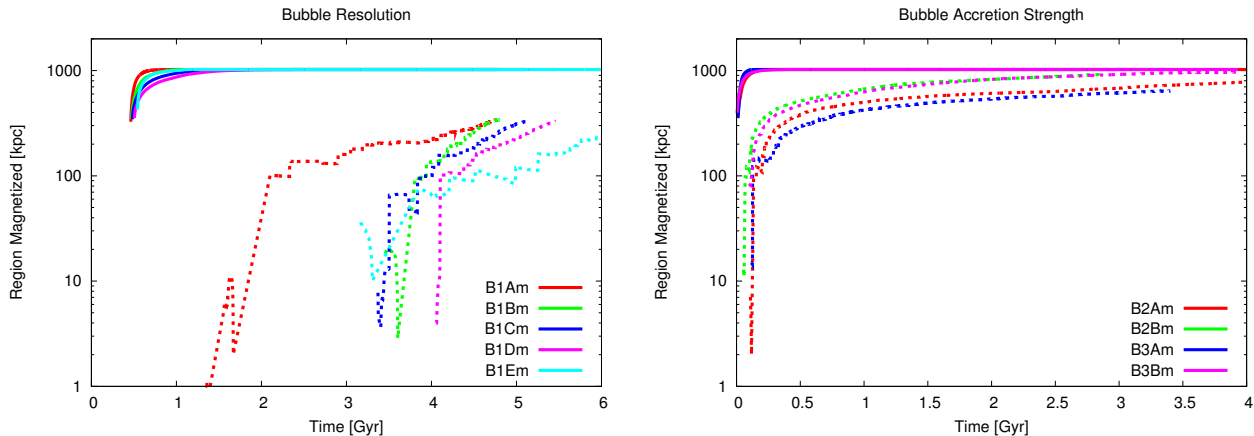


Figure 25. Affecting the volume magnetized by varying the bubble model parameters. Shown is the cube root of the total volume containing fields of strength at least 10^{-12} G (solid lines) and 10^{-6} G (dotted lines).

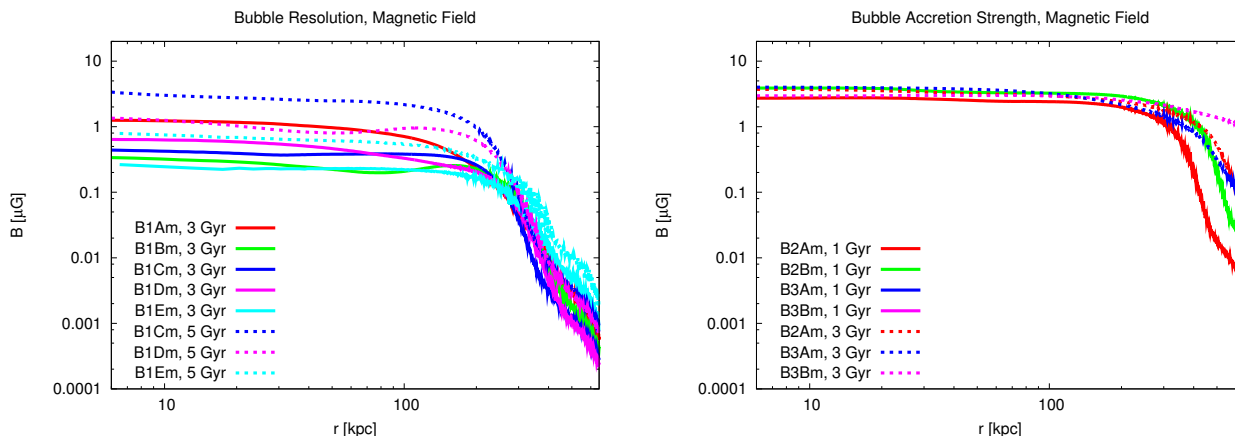


Figure 26. Affecting the magnetic profiles by varying the bubble model parameters. Shown are volume-weighted magnetic fields as a function of radius.

of magnetic fields, we do not have enough spatial or temporal resolution to fully study the evolution of a single bubble. In general, strong magnetic fields placed near the central black hole are very effective at pushing gas away from the core and preventing cooled gas from accreting.

All models quickly permeate the entire cluster with fields of strength greater than 10^{-12} G and produce strong fields ($> 10^{-6}$ G) in the central core. While jets produce slightly stronger fields in the innermost regions of the cluster, the bubbles more quickly disperse relatively strong fields out to larger radii. Additionally, the bubble models produce flat radial profiles out to ~ 300 kpc, beyond which the field strength drops rapidly. Although the jets produce steeper radial profiles, they can take up to 4 Gyr to sufficiently magnetize the inner regions of the cluster.

The jets and fixed bubbles maintain regular torus-like shapes in the magnetic field that persist over several billion years with strong fields concentrated in the core, although eventually the fixed bubbles begin to disperse. While we did not explicitly calculate correlation lengths, all of our models produce field lines which are not sufficiently tangled. Thus, if we are to consider the jet or fixed bubble subgrid models as realistic approaches, we must require some exter-

nal source of turbulence to tangle the generated magnetic fields. For example, galaxy wakes, which can amplify seed fields in less than 5 Gyr (Subramanian et al. 2006), can easily tangle the magnetic fields produced even at early times. Also, observations suggest that jets can precess (e.g. Storchi-Bergmann et al. 1997; Caproni & Abraham 2004), which would naturally lead to more tangled fields. The randomly-placed bubbles immediately produce large-scale highly tangled magnetic fields out to relatively large radii. However, the bubbles have difficulties generating magnetic fields with strength greater than a microGauss, something that is relatively easily to accomplish with the fixed bubbles and especially the jets.

We found the jet models to be relatively insensitive to many changes in the underlying model. Since the jets require high resolution in the first place (i.e., < 1.0 kpc) further improvements to the resolution leave the jet outflow properties unchanged. We found that it is necessary to keep the accretion radius smaller than the injection region size, but changes to the depletion radius are less important since the accretion rate is so low. We see the biggest differences in the jet outflows when changing jet size. On the other hand, changing the accretion strength parameter has little

effect, since stronger jet outflows simply push more gas away from the black hole, reducing the measured accretion rate to nearly its value in the fiducial case.

The bubble models are much more sensitive to changes in the accretion strength parameter, since the injection region is much larger. Even though increasing α is generally used to compensate for lower resolution, we found that the combination of lower resolution with enhanced α do *not* mimic the behavior of a higher resolution simulation with lower accretion strength parameter. Higher values of α lead to very large, rapidly-forming bubbles. Thus, we advise caution when choosing a value for α , especially when considering magnetic feedback subgrid models. A value of α chosen to match, for example, the observed $M_{\text{bh}} - \sigma$ relation may produce unrealistic bubbles. Furthermore, for this particular cluster, which has a relatively flat inner density profile, we only began to see significant differences when lowering the resolution past ~ 4 kpc. Mature cool-core clusters, more typically studied in isolated simulations, have steeper inner radial density profiles, and thus we expect to see a stronger dependence on α . However, this cluster represents a younger cluster, before it has developed a cool core, and better represents a typical cluster when AGN activity first begins seeding magnetic fields in its atmosphere.

While the jets appear to be more robust, they have significant difficulties in quickly and efficiently magnetizing the cluster. They must require some additional mechanisms operating in the intracluster medium to spread and tangle the injected fields. On the other hand, the randomly-placed bubbles, which automatically generate rich, tangled magnetic field morphologies, are more sensitive to subgrid model choices. Additionally, our fiducial case - with parameters taken directly from Sijacki et al. (2007) - produces very large bubbles very rapidly, which suggests that this model is not appropriate for general cluster atmospheres. Since the fixed bubbles have a predetermined radius they do not face this problem. While they also produce somewhat ordered fields, they spread these fields out to larger volumes, which makes these fields more susceptible to tangling from cluster mergers and galaxy motions. They can also strongly magnetize the cluster very quickly - in less than 1 Gyr.

While we have performed a relatively exhaustive analysis, many questions remain. The diversity of the model behavior exhibited under our analysis suggests significant theoretical uncertainty in the effects of AGN-based magnetic fields - we must carefully select subgrid models such that they reproduce cluster observables as well as faithfully represent the unresolved scales and physics. To achieve this, these magnetic field models must be tested in more realistic clusters to determine their ability to sufficiently magnetize the clusters absent any assumptions about the strength of the injected magnetic fields. Secondly, we must use these resimulated clusters to more fully evaluate these magnetized outflows in terms of observables, such as AGN duty cycle and cluster X-ray surface brightness profiles. We must study more topologies of magnetic injection, such as random fields, to determine if the resulting magnetic outflows are robust against changes to the injected field structure. Finally, we must perform fully cosmological simulations to ensure that the given AGN subgrid models, when injected magnetic fields are included, reproduce key observables, such as the relationship between supermassive black hole mass and host

galaxy bulge velocity dispersion. Only then can we be confident that our magnetic subgrid models accurately represent realistic aspects of AGN evolution, and use them to evaluate the ability of active galactic nuclei to generate cluster-wide magnetic fields.

ACKNOWLEDGMENTS

The authors acknowledge support under a DOE Computational Science Graduate Fellowship (DE-FG02-97ER25308) and a Presidential Early Career Award from the U.S. Department of Energy, Lawrence Livermore National Laboratory (contract B532720). Computing resources were supplied by an allocation provided by the National Science Foundation (TG-AST040034N) on Kraken at the National Institute for Computational Sciences, as well as the Oak Ridge Leadership Computing Facility at the Oak Ridge National Laboratory, which is supported by the Office of Science of the U.S. Department of Energy under Contract No. DE-AC05-00OR22725. The software used in this work was in part developed by the DOE-supported Flash Center for Computational Science at the University of Chicago. Visualizations were created using the DOE-supported VisIt program.

REFERENCES

- Allen, S. W., Dunn, R. J. H., Fabian, A. C., Taylor, G. B., & Reynolds, C. S. 2006, MNRAS, 372, 21
- Balbus, S. A. 2000, ApJ, 534, 420
- . 2001, ApJ, 562, 909
- Bamba, K., Ohta, N., & Tsujikawa, S. 2008, Phys. Rev. D, 78
- Bandara, K., Crampton, D., & Simard, L. 2009, ApJ, 704, 1135
- Battaglia, N., Bond, J. R., Pfrommer, C., Sievers, J. L., & Sijacki, D. 2010, ApJ, 725, 91
- Battfeld, D., Battfeld, T., Wesley, D. H., & Wyman, M. 2008, JCAP, 2, 1
- Baym, G., Bödeker, D., & McLerran, L. 1996, Phys. Rev. D, 53, 662
- Biermann, L. 1950, Zeitschrift Naturforschung Teil A, 5, 65
- Bondi, H. 1952, MNRAS, 112, 195
- Booth, C. M. & Schaye, J. 2009, MNRAS, 398, 53
- Brunetti, G., Venturi, T., Dallacasa, D., Cassano, R., Dolag, K., Giacintucci, S., & Setti, G. 2007, ApJ, 670, L5
- Caproni, A. & Abraham, Z. 2004, ApJ, 602, 625
- Carilli, C. L. & Taylor, G. B. 2002, ARA&A, 40, 319
- Cattaneo, A. & Teyssier, R. 2007, MNRAS, 376, 1547
- Chandran, B. D. G. & Maron, J. L. 2004, ApJ, 602, 170
- Colbert, E. J. M., Baum, S. A., Gallimore, J. F., O’Dea, C. P., & Christensen, J. A. 1996, ApJ, 467, 551
- Colgate, S. A. & Li, H. 2000, 195, 255
- Contopoulos, I., Christodoulou, D. M., Kazanas, D., & Gabuzda, D. C. 2009, ApJ, 702, L148
- Daly, R. A. & Loeb, A. 1990, ApJ, 364, 451
- Debuhr, J., Quataert, E., Ma, C.-P., & Hopkins, P. 2010, MNRAS, 406, L55
- Di Matteo, T., Colberg, J., Springel, V., Hernquist, L., & Sijacki, D. 2008, ApJ, 676, 33

- Dolag, K. & Schindler, S. 2000, *A& AP*, 364, 491
- Dubey, A., Reid, L. B., & Fisher, R. 2008, *Physica Scripta*, T132, 014046
- Dubois, Y., Devriendt, J., Slyz, A., & Silk, J. 2009, *MNRAS*, 399, L49
- Dubois, Y., Devriendt, J., Slyz, A., & Teyssier, R. 2010, *MNRAS*, 409, 985
- Dubois, Y., Devriendt, J., Slyz, A., & Teyssier, R. 2011, *ArXiv e-prints*
- Dursi, L. J. & Pfrommer, C. 2008, *ApJ*, 677, 993
- Falceta-Gonçalves, D., Caproni, A., Abraham, Z., Teixeira, D. M., & de Gouveia Dal Pino, E. M. 2010a, *ApJ*, 713, L74
- Falceta-Gonçalves, D., de Gouveia Dal Pino, E. M., Gallagher, J. S., & Lazarian, A. 2010b, *ApJ*, 708, L57
- Fan, X. 2006, *New Astronomy Reviews*, 50, 665
- Fender, R. et al. 1999, *ApJ*, 519, L165
- Fryxell, B. et al. 2000, *ApJs*, 131, 273
- Gallo, E., Fender, R. P., & Pooley, G. G. 2003, *MNRAS*, 344, 60
- Gardini, A. 2007, *A&A*, 464, 143
- Gaspari, M., Melioli, C., Brighenti, F., & D’Ercole, A. 2011, *MNRAS*, 411, 349
- Gourgouliatos, K. N., Braithwaite, J., & Lyutikov, M. 2010, *MNRAS*, 409, 1660
- Hopkins, P. F., Narayan, R., & Hernquist, L. 2006, *ApJ*, 643, 641
- Jones, T. W. & De Young, D. S. 2005, *ApJ*, 624, 586
- Kirkpatrick, C. C., McNamara, B. R., & Cavagnolo, K. W. 2011, *ApJ*, 731, L23+
- Koide, S., Shibata, K., & Kudoh, T. 1999, *ApJ*, 522, 727
- Lesch, H. & Birk, G. T. 1998, *Physics of Plasmas*, 5, 2773
- Li, H., Lapenta, G., Finn, J. M., Li, S., & Colgate, S. A. 2006, *ApJ*, 643, 92
- McNamara, B. & Nulsen, P. 2007, *ARA&A*, 45, 117
- Miniati, F., Jones, T. W., Kang, H., & Ryu, D. 2001, *ApJ*, 562, 233
- Morsony, B. J., Heinz, S., Brügggen, M., & Ruszkowski, M. 2010, *MNRAS*, 407, 1277
- Narayan, R. & Medvedev, M. V. 2001, *ApJ*, 562, L129
- Navarro, J. F., Frenk, C. S., & White, S. D. M. 1996, *ApJ*, 462, 563
- O’Neill, S. M. & Jones, T. W. 2010, *ApJ*, 710, 180
- Parrish, I. J., Quataert, E., & Sharma, P. 2009, *ApJ*, 703, 96
- Peterson, J. & Fabian, A. 2006, *Physics Reports*, 427, 1
- Pfrommer, C., Enßlin, T. A., Springel, V., Jubelgas, M., & Dolag, K. 2007, *MNRAS*, 378, 385
- Pope, E. C. D. 2007, *MNRAS*, 381, 741
- Robinson, K. et al. 2004, *ApJ*, 601, 621
- Ruszkowski, M., Enßlin, T. A., Brügggen, M., Heinz, S., & Pfrommer, C. 2007, *MNRAS*, 378, 662
- Shukurov, A., Subramanian, K., & Haugen, N. E. L. 2006, *Astronomische Nachrichten*, 327, 583
- Sijacki, D., Springel, V., Di Matteo, T., & Hernquist, L. 2007, *MNRAS*, 380, 877
- Skillman, S. W., O’Shea, B. W., Hallman, E. J., Burns, J. O., & Norman, M. L. 2008, *ApJ*, 689, 1063
- Sternberg, A., Pizzolato, F., & Soker, N. 2007, *ApJ*, 656, L5
- Sternberg, A. & Soker, N. 2008, *MNRAS*, 389, L13
- Storchi-Bergmann, T., Eracleous, M., Ruiz, M. T., Livio, M., Wilson, A. S., & Filippenko, A. V. 1997, *ApJ*, 489, 87
- Subramanian, K., Shukurov, A., & Haugen, N. E. L. 2006, *MNRAS*, 366, 1437
- Sutherland, R. S. & Dopita, M. A. 1993, *ApJS*, 88, 253
- Sutter, P. M. & Ricker, P. M. 2010, *ApJ*, 723, 1308
- Voit, G. M. & Donahue, M. 2005, *ApJ*, 634, 955
- Widrow, L. 2002, *Reviews of Modern Physics*, 74, 775
- Xu, H., Li, H., Collins, D., Li, S., & Norman, M. L. 2008, *ApJ*, 681, L61
- Xu, H., Li, H., Collins, D. C., Li, S., & Norman, M. L. 2010, *ApJ*, 725, 2152
- Yang, H.-Y., Sutter, P., & Ricker, P. 2011, *ApJ* (submitted)